EFFECT OF L-ARGININE CONJUGATED CARBON NANOTUBE (CNT) REINFORCED SULFONATED POLYETHER ETHER KETONE (SPEEK) NANOFILMS ON CELL PROLIFERATION

by

Hatice Kaya

B.Sc., Bioengineering, Yıldız Technical University, 2013

Submitted to the Institute of Biomedical Engineering
in partial fulfillment of the requirements
for the degree of
Master of Science
in
Biomedical Engineering

Boğaziçi University
2017

ACKNOWLEDGMENTS

First, I would like to express my deep gratitude to my research advisor, Asist. Dr. Duygu EGE, for her precious advice, supports and supervision throughout my graduate experience.

I am grateful to Assoc. Prof. Dr. Bora Garipcan and his research group members for their contributions. I would also like to thank Assist. Prof. Dr. Osman Bulut for helping us to conduct the mechanical analysis and for his advice as well.

I would like thank to BoNerve group members, Ilayda Duru, Öznur Demir Can, Morteza Teymoori, and Sepideh Tavakoli for the harmony in the group and constructive discussion.

I want to express my gratitude to my friends Seher Dağtekin Yaray, Fatma Zehra Erkoç, Hayriye Öztatlı, Sabra Rostami and Alp Özgün for both their friendship, motivation and scientific supports during thesis processes. It would be pretty hard to carry all the stress of thesis process without them.

I would like to thank my beloved husband Serkan Kaya for his respect, patience and love not only in the thesis preparation period but also in all time that we live together.

I can find no words to express gratitude to my mother Hayriye Oruçoğlu, my brothers Murat and Mithat Oruçoğlu and my sisters Döndü Ayvalık and Safa Oruçoğlu for their unconditional love and supports in every stage of my life.

ACADEMIC ETHICS AND INTEGRITY STATEMENT

I, Hatice Kaya, hereby certify that I am aware of the Academic Ethics and Integrity Policy issued by the Council of Higher Education (YÖK) and I fully acknowledge all the consequences due to its violation by plagiarism or any other way.

Name :

Signature:

Date:

ABSTRACT

EFFECT OF L-ARGININE CONJUGATED CARBON NANOTUBE (CNT) REINFORCED SULFONATED POLYETHER ETHER KETONE (SPEEK) NANOFILMS ON CELL PROLIFERATION

Poly ether ether ketone (PEEK) exhibits distinct properties which are favorable in designing a novel load-bearing implant for bone reconstruction. It overcomes the adverse effects of metallic implants such as stress shielding, release of toxic ions and radiotherapy interference. PEEK has comparatively closer elastic modulus to that of cortical bone than metallic implants, which in turn prevents stress shielding and subsequent bone resorption. Furthermore, elastic modulus of PEEK is tunable by incorporation of additives. However, hydrophobic bioinert surface of PEEK which are not favorable for cell adhesion brings about some limitations in its application due to inefficient osseointegration. Furthermore, although the addition of fillers promote the mechanical attributes, PEEK nanocomposite might be still insufficient regarding inducement of bioactivity. Many studies show that presence of L-arginine (L-Arg) assists cell attachment and proliferation. In this thesis, functionalized multi-walled carbon nanotubes (f-MWCNT) reinforced sulphonated poly ether ether ketone (SPEEK) was fabricated by solvent casting. Previously, PEEK was dissolved in high concentric sulfuric acid (H_2SO_4) to gain SPEEK and MWCNT was oxidized with mixing of sulfuric acid (H_2SO_4, 98%) and nitric acid (HNO_3, 65%) to obtain carboxyl groups on the sidewall and ends of MWCNT. The surface of the obtained nanofilms were covalently conjugated with L-arginine. The samples were characterized with Proton Nuclear Magnetic Resonance Spectroscopy (H-NMR), Fourier Transform Infrared Spectroscopy (FTIR), X-ray Photoelectron Spectroscopy (XPS), Water Contact Angle (WCA) measurement, Atomic Force Microscope (AFM) and Dynamic Mechanical Analysis (DMA).Finally, impact of CNT and L-arg existence on cellular response was analyzed using human fetal osteoblast (hFOB) via Alamar blue test. The chemical characterization of surface with FTIR and H-NMR, functional sulfur and carboxyl groups formed were confirmed. Immobilization of L-Arg was confirmed via XPS showing the Nitrogen (N) atom presence

and chemical state of N atom. The mechanical strength of nanofilms were improved which was proven by DMA. Cell viability was observed the highest for L-arg grafted nanofilm. In conclusion, this study indicates that arginine modified CNT/PEEK films are promising candidates for femoral replacement applications.

Keywords: PEEK, MWCNT, Solvent casting, Surface modification, L-arginine, Cortical bone.

ÖZET

L-ARJİNİN BAĞLI KARBON NANOTÜP (KNT) TAKVİYELİ SÜLFONATLANMIŞ POLİ ETER ETER KETON (SPEEK) NAFİLMLERIN HÜCRE ÇOĞALMASINA ETKİSİ

Poli eter eter keton (PEEK), kemik rekonstrüksiyonu için yük taşıyıcı implant tasarımına uygun özelliklere sahiptir. Termoplastik bir polimer olan PEEK gerilim koruması, toksik iyonların serbest salınımı ve radyoterapi etkileşimi gibi metalik implantların olumsuz etkilerini ortadan kaldırabilecek potansiyel bir malzemedir. Metalik implantlara kıyasla PEEK kortikal kemiğe daha yakın elastik modülüne sahiptir; bu da gerilme korumasını ve dolayısıyla kemik rezorpsiyonunu önler. Ayrıca, PEEK'in elastik modülü takviye malzemesi ile ayarlanabilir. Fakat zayıf osseoentegrasyon nedeniyle PEEK'in biyoinert yüzeyi uygulamasında sınırlamalara yol açmaktadır. Ayrıca, katkı maddesi eklenmesi mekanik özellikleri geliştirmesine rağmen PEEK nanokompozit biyokativiteyi artırma yönünden yetersiz kalabilmektedir. Birçok çalışma, malzemenin yüzeyinde L- arjinin (L-arg) bulunması hücre yapışmasına ve çoğalmasına yardımcı olduğunu göstermiştir. Bu tez çalışmasında, fonksiyonlanmış çok duvarlı karbon nanotüp (f-ÇDKNT) takviyeli sulfonatlanmış PEEK (SPEEK) çözücü döküm yontemiyle üretilmiştir. öncelikle, SPEEK elde etmek için PEEK yüksek konsantrasyonlu sülfürik asit (H_2SO_4) içinde çözülmüştür ve ÇDKNT'ün yan duvarlarına karboksil grupları bağlamak için ÇDKNT sülfürik asit ($H_2SO_4, 98\%$) ve nitrik asit ($HNO_3, 65\%$) karışımı ile oksitlenmiştir. Sonrasında, elde edilen nanofilmlerin yüzeyine, L-arjinin kovalent olarak bağlanmıştır. Numuneler Proton Nükleer Manyetik Rezonans Spektroskopisi (H-NMR), Fourier Dönüşümü Kızılötesi Spektroskopi (FTIR), X-ışını Fotoelektron Spektroskopisi (XPS), Su Temas Açısı (WCA), Atomik Kuvvet Mikroskopu (AFM) ve Dinamik Mekanik Analiz (DMA) yöntemleriyle karakterize edildi.Son olarak, L-arg ve KNT varlığının hücre tepkisi üzerindeki etkisi Alamar Blue testi ile human fetal osteoblast (hFOB) kullanılarak analiz edilmiştir.FTIR ve H-NMR ile fonksiyonel sülfür ve karboksil gruplarının bulunduğunu kanıtlamıştır. Bununla birlikte, film yüzeyine L-arg immobilizayonu XPS analizi ile doğrulandı ve yüzey araştırma spektrum ve yüksek

çözünürlükteki azot piki sırasıyla azot atomunun varlığını ve nitrojen atomunun yapıdaki kimyasal bağ düzenini göstermiştir. f-ÇDKNT takviyesiyle nanofilmlerin mekanik özelliklerinde iyileşmenin olduğu DMA analizi ile ispatlanmıştır.Hücre canlılığının en çok L-arg da olduğu gözlenmiştir. Sonuç olarak, bu çalışma arjinin ile modifiye edilmiş KNT/PEEK filmlerinin femur implant uygulamaları için umut verici olduğunu göstermiştir.

Anahtar Sözcükler: PEEK, MWCNT, solvent dökümü, yüzey modifikasyonu, L-arjinin, Kortikal Kemik.

TABLE OF CONTENTS

LIST OF FIGURES

LIST OF TABLES

LIST OF SYMBOLS

H_2SO_4	Sulfuric Acid
HNO_3	Nitric acid
E'	Storage modulus
Tg	Glass transition

LIST OF ABBREVIATIONS

PEEK	Poly ether ether ketone
SPEEK	Sulphonated poly ether ether ketone
L-Arg	L-arginine
CNTs	Carbon nanotubes
f-MWCNT	Functionalized multi-walled carbon nanotubes
H-NMR	Proton Nuclear Magnetic Resonance Spectroscopy
FTIR	Fourier Transform Infrared Spectroscopy
XPS	X-ray Photoelectron Spectroscopy
WCA	Water Contact Angle
AFM	Atomic Force Microscope
DMA	Dynamic Mechanical Analysis
hFOB	human fetal osteoblast
SWCNTs	Single-walled carbon nanotube
DWCNTs	Double-walled carbon nanotubes
MWCNTs	Multi-walled carbon nanotube
vdW	Strong van der Waals
PTFE	Polytetrafluoroethylene
GA	Glutaraldehyde
C	Carbon
O	Oxygen
N	Nitrogen
DS	Degree of sulfonation
TCP	Tissue culture plate

1. INTRODUCTION

1.1 Motivation

The metallic implants are considered as the gold standard in orthopedic applications. However, some adverse effects might arouse due to release of toxic ions, prevention of post operation imaging, and its stress shielding effect [1]. Stress shielding effect results from mismatch of elastic modulus of implant and bone tissue which leads to losing bone tissue adjacent the implant material [2]. Researches on development of isoelastic implantable biomaterial with comparable mechanical strength with that of bone are gaining interest. The growing interest to replace thermoplastic polymers with metallic counterparts has been especially due to high performance of thermoplastic polymers [3, 4].

Poly ether ether ketone (PEEK) is a rigid semicrystalline high performance engineered polymer and it is becoming a popular biomaterial for production of orthopedic implants such as spinal interbody fusion cages due to its high wear resistance, corrosion resistance and biocompatibility [5, 6]. The elastic modulus of PEEK (3.7 GPa) comparable with bone tissue Moreover, radiolucent properties of PEEK enables X-ray imaging and repeated sterilization [6]. Aforementioned attributes render PEEK a potential candidate for substitution of metallic orthopedic implants in long term application.

Although PEEK is regarded as mostly capable of meeting the requirements of bone implants, it is bioinert and hydrophobic which are not favorable when direct contact is crucial between bone tissue and implantable material [7]. There are four fundamental factors which should be taken into account to determine the biocompatibility of the implants once the implant needs to be in direct contact with bone tissue. These factors are as follows: surface composition, surface energy, surface roughness and surface topography [8]. Surface coating, chemical modification and the addition

of various additives into PEEK was practiced to improve the biological performance of PEEK by facilitating cell adhesion and growth [9].

In comparison to other carbon based fillers, carbon nanotubes (CNTs) are effective even at relatively low concentrations owing to its high surface area stemmed from its high aspect ratio. Extraordinary high strength, toughness and elastic modulus of multi-walled carbon nanotubes (MWCNTs) associated with their distinct structural characteristics render that material appealing for reinforcing polymeric matrix by obtaining an advanced nanocomposite material with superior mechanical properties than that of the neat polymer [10]. Tensile strength of MWCNTs reaches up to 150 GPa and the Young's modulus of MWNTs is approximately 0.95 TPa [11]. Fabricated novel nanocomposite with the improved mechanical properties could be favorable for load-bearing orthopedic application.

Although CNTs enable achievement of remarkable properties to their nanocomposites they are inclined to form bundles in common solvents which in turn prevents their effective use in the biomedical applications [12]. Covalent and noncovalent functionalization strategies make CNTs soluble by preventing agglomeration of CNT particles due to strong van der Waals forces.

In order to improve the biological activity of CNT/PEEK nanocomposites, the surface of biomaterials can be coupled with biomolecules. L-arginine is a strong candidate for surface functionalization of PEEK as it has many biological properties such as being an anticoagulant, promotion of angiogenesis, wound healing, cell growth and finally it also induces interaction of circulatory blood cells with the vessel wall [13, 14, 15].

Literature survey showed that there are several researches concerning surface modification of PEEK or carbon based PEEK to accomplish a favorable environment cell attachment and growth, because enhanced bioactivity of material allow it usage where promotion of forming bone tissue is necessary at the defect side.

In this regard, the aim of this study is to develop bioactive surface for PEEK/CNT

nanocomposite film via immobilization of L-arginine to promote the cell attachment and cell proliferation in bone-implant interface of load-bearing biomedical applications, thus overcoming the insufficient osseointegration.

1.2 Objectives

In the scope of this master dissertation, the aim is to fabricate CNT/PEEK nanocomposites with enhanced osseointegration through L-Arg modification of the surface, to be employed as a long-term implantable orthopedic material.
The main objectives of this study are as follows:

- To increase solubility of PEEK via sulfonation reaction.
- To functionalize the CNT for enhancement of interface adhesion with polymer.
- To investigate the effect of CNT concentration on mechanical and wettability properties of the nanocomposite film.
- To immobilize the L-arginine on the surface of nanofilm and examine the effect of L-arginine on the cell adhesion and proliferation

1.3 Outline

This thesis is composed of 5 chapters, which are presented consecutively. Chapter 1 is an introduction. Chapter 2 is an introduction to bone's structure, femur fracture, modification of PEEK, application of PEEK in the medical field, CNT functionalization and nanocomposite fabrication methods. The procedures for experimental studies are described in the Chapter 3, which follows with the results section in Chapter 4. Finally, in Chapter 5, the thesis is concluded with discussion of results, conclusion and suggestion for future works.

2. BACKGROUND

2.1 Bone Structure

Bone is one of the fundamental components of the skeletal system. Unlike the other tissues bone is more rigid and hard. However it has not a homogeneous structure. Cortical and spongy bone can be seen as a transversely and orthotropic materials, respectively. The compression strength of bone tissue is much stronger than tension strength, and has much greater Young's Modulus than shear modulus. The bone is composed of two types of structures at the macroscopic scale. They are named as cortical (compact or Haversian) and cancellous (spongy, or trabecular) bone. The compact bone has higher density. Cortical bone corresponds to about 80% of the skeletal mass, which forms the bone outer wall and supports and protects function of the skeleton. Osteon is the major unit of the cortical bone. A typical shape of osteon is a hollow cylindrical with the outer and inner diameters of about 200 μm and 50 μm, respectively. Otherwise, cancellous bone is composed of a narrow lattice rods and plates (70 to 200 μm in thickness) called trabeculae. The trabeculae are encircled by bone marrow that is vascular and transport nutrients and takes away its waste disposal [16].

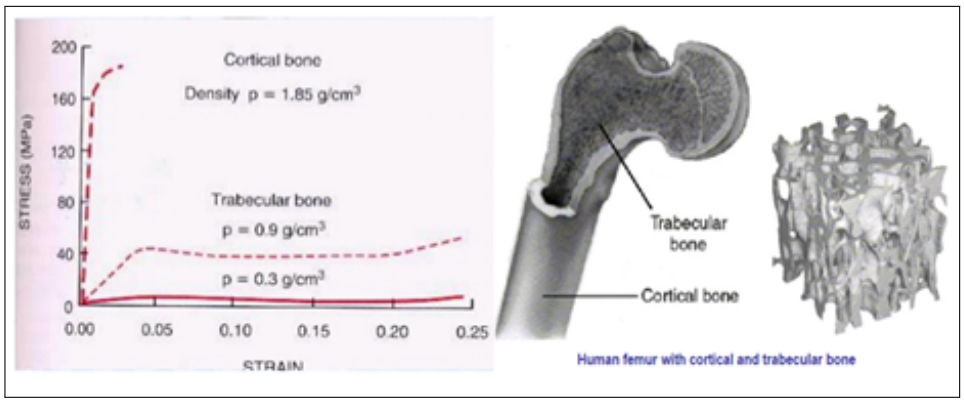

Figure 2.1 The mechanical properties between trabecular and cortical bone.

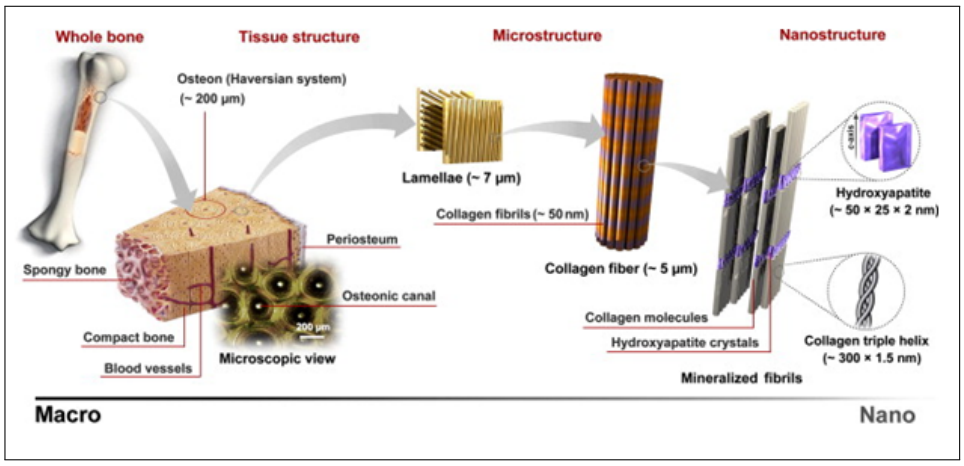

Figure 2.2 Depicts the hierarchical organization of human cancellous bone from the nano- to the macroscale.

2.1.1 Femur Fracture

Dynamic tissue like bone has a fundamental function which is to carry load and support and protect organs. When a fracture caused by a serious injury or trauma occurs, the transmission of normal forces through the bone is disrupted. Treatment of fractures aims at achieving a situation as close to the prefracture situation as possible [17].

Femur (thighbone) is the longest and strongest bone in the body. Because the femur is so strong, it usually takes a lot of force to break it. Femoral fractures in young people are frequently due to some type of high-energy collision. For example car crashes are the number one cause of femur fractures [17].

2.1.2 Types of Femoral Shaft Fractures

There four types of fracture including transverse, oblique, comminuted and spiral. Transverse fracture is a straight horizontal line going across the femoral shaft. On the other hand oblique fracture is angled fracture across shaft. The fracture line encircles the shaft when spiral fracture occurs. Finally, Comminuted fracture is the fracture of bone breaks into two or many pieces [17].

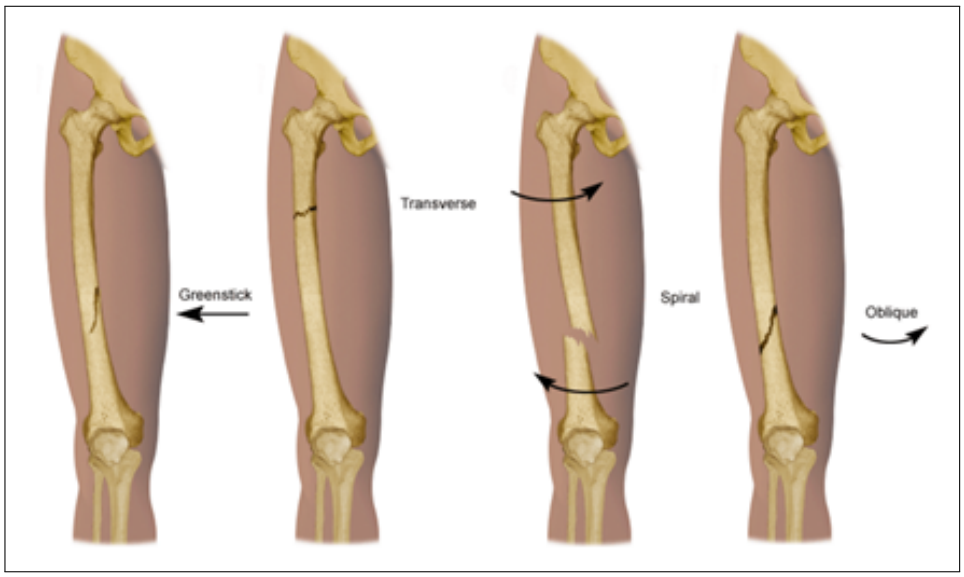

Figure 2.3 Representation of femur bone fracture.

2.2 Poly (Ether ether ketone) (PEEK)

Polyether ether kethone (PEEK) is an organic thermoplastic polymer in a semi-crystalline structure. PEEK is known as high performance engineering material with prominent mechanical strength. Its great mechanical properties are associated with the symmetry of benzene rings along the linear polyaromatic polymer backbone which is consisting of two ether groups and a kethone group [18].

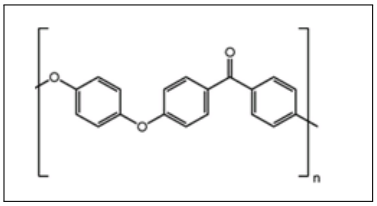

Figure 2.4 Chemical structure of PEEK.

PEEK has an extreme resistance to chemicals, electricity, radiation and temperature. Due to the fact that PEEK maintains structural stability at temperatures greater than 300°C, this material can be handled easily without dimensional alterations. In addition of processability of PEEK, it is non-cytotoxic and can be repeatedly sterilized using conventional steam, γ-irradiation and ethylene oxide treatment without any deterioration of its mechanical properties [19].

PEEK is considered an advanced biomaterial for medical implants to supply structural support or to substitute with bone tissue . In contrast to Ti and its alloy, elastic modulus of PEEK is lower and closer to that of human cortical bone. This can prevent the effect of stress shielding causes bone resorption around biomaterial after implantation process. In addition to noticable mechanical properties, thermal stability, chemical resistance, biocompatibility, good wear resistance and natural radiolucency make PEEK favorable biomaterial to apply in orthopedic implants especially for load-bearing bone tissue engineering.

Besides all the merits of PEEK, the reason why PEEK does not to release toxin ion, by product and not to corrode or degrade is that PEEK generally has inactive biological surface (bioinert) owing to chemically stable structure. Hydrophobic surface of PEEK results in a low surface energy which arouses adverse osseointegration. Restricted cell adhesion underlies insufficient bone-implant contact [2]. Bioactivity which means positive interaction between biomaterial and biological environment at the defected side should be taken into consideration and must be improved not to cause any inflammation during wounds healing process [5]. Topological and chemical factors of biomaterials must be modified or coated in order to increase bioactivity so that the response of tissue against the biomaterial and the wound healing process associated with compatibility between implant and bone tissue is mitigated. Surface modification of biomaterials could be effective approach to augment the growth of cells and their adhesion on the surface which means an enhanced robust bone-implant integration.

It has been reported that hydrophilic surface of material contributes to cell adhesion and cell proliferation. A hydrophilic surface can be obtained by adjusting with hydrophilic functional groups, peptides or amino acid molecules which in turn promote the chemical activitiy of the suface and cell growth as well [2].

Many efforts have been made to devolop the properties of the neat PEEK thoruogh an incooperation with fillers such as carbon fibres,glass fibres and carbon nanotubes [20]. The first study on polymer nanocomposites using carbon nanotubes as fillers were introduced by Ajayan et al. in 1994 [11]. Since then a profound investi-

gations have been conducted about incorporation of CNT into the polymer matrix to accomplish excellent properties in contrast to the bare polymer. Recently, In addition to several methods applied for manufacturing CNTs/PEEK, it also was taken attention on that further studies on CNT-based PEEK composites need to be conducted to understand cellular behavior and the mechanism of bone tissue formation [19].

2.3 Carbon Nanotubes (CNTs)

Carbon nanotubes (CNTs) first were discovered by the Japanese electron microscopist Sumio Iijima in 1991. Because of its potential structural application many scientists give attention CNTs' unique properties caused by its rigid atomic structure [21]. They have emerged as a promising nanomaterial owing to their tremendous combination of strength, ultra-light weight, high surface area and high stability, which allow them to employ for composite reinforcement material in biomedical field [22].

2.3.1 Structure of CNTs

Carbon nanotubes (CNTs) are allotropes of carbon with a cylindrical nanostructure were first introduced by Iijima et al. almost two decades ago. The formation of this novel artificial nanomaterial resembles the rolling of a graphene sheet constructed from exclusively the sp^2 hybridized carbon atoms in a hexagonal lattice constitutes hollow cylinders as shown in the Figure 2.5. While its diameter is changing in nano-metric scale, the length of CNTs is ranging from a few nanometers to several microns. The number of concentric cylinders determines the type of CNT. According to the intensity of concentric cylinders mainly three types of CNT exist, which are single-walled carbon nanotube (SWCNTs), double-walled carbon nanotubes (DWCNTs) and multi-walled carbon nanotube (MWCNTs) as shown in the Figure 2.6 [23].

SWCNTs consist of a single graphene layer rolled up into a seamless cylinder and their diameters is ranging from 0.4 to 2 nm. The structure of SWCNTs can be

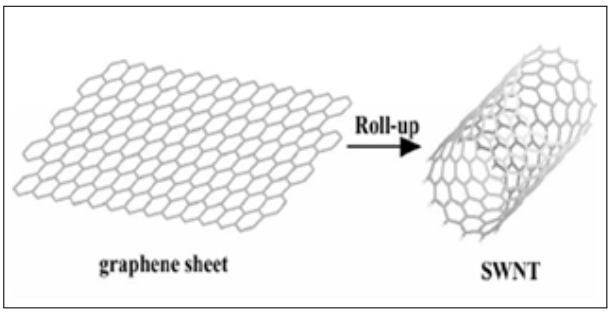

Figure 2.5 Visualization of CNT formation from graphene flakes [24].

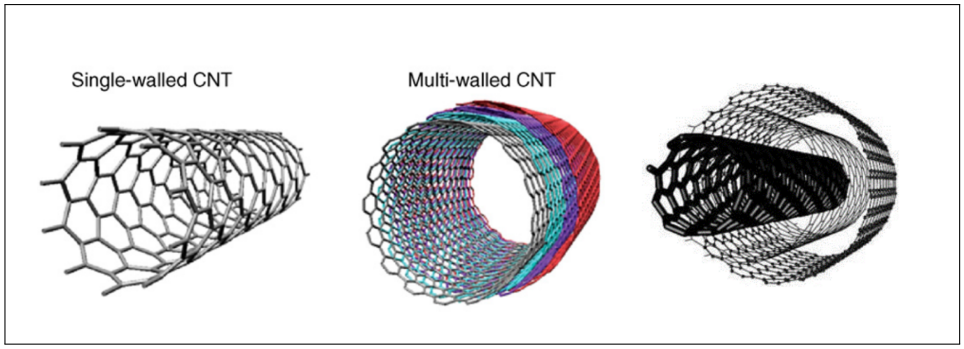

Figure 2.6 Different type of CNTs which based on the number of tubes walls [25].

differentiated through its chiral vector occurred by how the graphene sheet is wrapped with different angles in hexagonal lattice lattice to create a seamless cylindrical tube. They are named as zigzag, armchair, chiral form of the SWCNTs, see the Figure 2.7.The electrical properties of CNTs are differed by chiral angle and diameter. It could show metallic behaviour (armchair CNTs) or similar to semiconducting (zigzag and chiral CNTs) materials' behavior. More than two concentric cylinders of graphene sheets form MWCNTS which are co-axially arranged around a central hollow core. The adjacent layers of graphene sheets are attracted to each other by van der Waals forces. Their diameters are in the range of 1-3 nm for the inner tubes and 2-100 nm for the outer tubes and length may reach up from 100 nm to several micrometres, respectively [26].

2.3.2 Properties of CNTs

CNTs are characterized with low density, high aspect ratio (long length compared to a small diameter) and high strength [28]. CNTs intrinsically exhibit unique

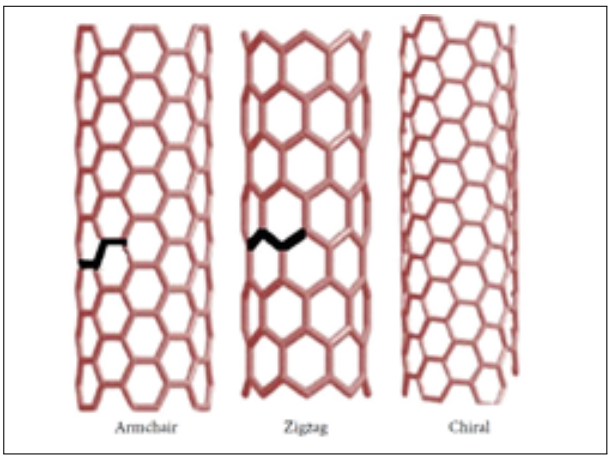

Figure 2.7 Configurations of Carbon nanotube structures of armchair, zigzag and chiral [27].

mechanical, thermal and electrical properties. The multi-faceted properties of the CNTs would originate in their atomic arrangement (or in other terms the way their graphene sheets are rolled). Their excellent mechanical characteristics are associated with the sigma bonds between individual carbon atoms (C-C bonding) in sp^2 hybridized CNTs. Elastic modulus of 1.2 TPa and tensile strength of about 50-200 GPa have been reported for CNTs [23].

2.3.3 Modification of CNT Surface

The conspicuous properties of CNT bestow to these materials a considerable potential to employ as a reinforcement agent in a host matrices to fabricate polymer nanocomposites with improved mechanical properties at very low concentration. When it comes to biomedical application of CNT there is some limitation of its usage. CNT structure is chemically inert. That makes processability of the crude CNT challenging. Moreover, the issue about dispersion of these nanoscale fillers homogeneously in the polymer matrix in order to offer sufficient interaction surface area for effective enhancement of the nanocomposite' properties are crucial. However, CNT is insoluble and its dispersibility is poor resulting from its innate highly hydrophobicity. That is to say CNTs' a great surface to volume ratio and strong van der Waals (vdW) forces in the CNT structure retain them together tightly, which give rise to composing of

large agglomerates which behave differently from individual CNTs. There is a difficulty in incorporating of pristine CNTs into polymer materials due to aforementioned entanglements. The formation of bundles in the polymer matrix results in reducing of interfacial adhesion between polymeric matrix and CNT filler, which adversely affects the load transfer. Therefore individual CNTs embedded in a polymer only exhibit a fraction of their potential. CNT aggregation has been found to dramatically hamper the mechanical properties of fabricated nanocomposites [23, 29]. There has been an immense effort to establish the most suitable conditions for the transfer of either mechanical (stress) load to individual nanotubes in a polymer composite component. A prerequisite for such an endeavor is the efficient dispersion of individual nanotubes and the establishment of a strong chemical affinity (covalent or non-covalent) with the surrounding polymer matrix. In order to surmount the obstacles, modification of CNTs' surface becomes essential via functionalization process. Attaching or wrapping several functional groups on the surface of CNTs encourage to exfoliate from bundles to give individual CNTs. Modifying has been reviewed to elevate CNTs' solubility and biocompatibility which are the most imperative factors taken into account for biomedical applications [25]. Moreover, the functionalization of CNT is a powerful way to hinder nanotube aggregation by promoting distribution of individual CNT tubes uniformly which lead to evolved adhesion of CNTs to miscellaneous host polymer matrix and advanced load transfer across the CNT-polymer interface successfully through good interfacial interactions as well.

Various methods for modification of CNT surface have been explored quite successfully in introducing functional moieties over CNT surface with reduced toxicity [30]. Strategies of functionalization can be divided into two categories which are non-covalent functionalization and covalent functionalization.

Having large hydrophobic aromatic (π-electron) of CNTs render them a eligible to interact with proper complementary molecules. Non-covalent functionalization (physical) of nanotubes can be carried out without any compromising of the physical properties of CNTs. Yet it is still capable of improving the solubility and processability of CNTs with polymer matrix. Weak physical interactions such as surface absorption,

electrostatic interactions, hydrogen bonding and π-π stacking are responsible for an effective attachment with large scale of molecules into CNT surface noncovalently (Figure 2.8, 2.9). Such interactions disrupt van der Waals forces which are caused CNTs to aggregate into bundles. This non-destructive approach basically includes coating with amphiphilic surfactant molecules and wrapping with long polymer chains as dispersing agents to obtain miscible CNT both in polymer matrix and compatible within biological systems. However, the shortcoming of the noncovalent functionalization is that the dispersion of CNTs is not stable which in turn; the suspension may reagglomerate after for a while [31, 32].

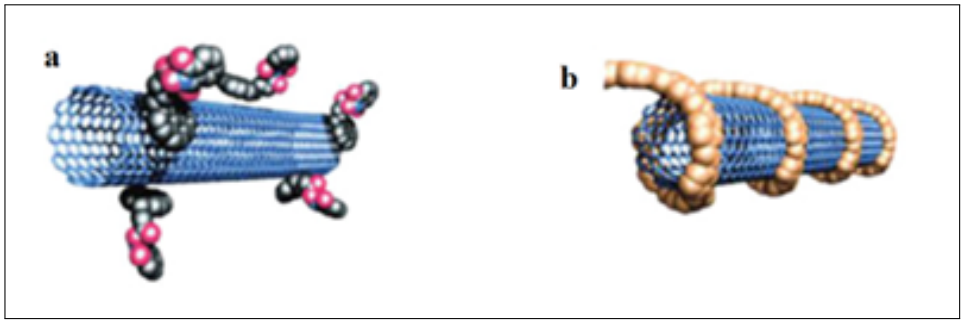

Figure 2.8 Noncovalent surfactant encapsulation (a) and polymer wrapping (b) [27].

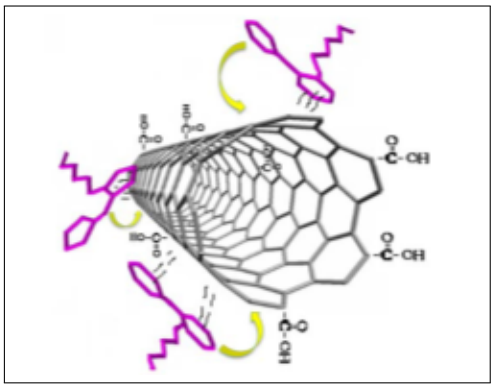

Figure 2.9 $\pi - \pi$ stacking interaction between single-walled carbon nanotube (SWCNT) and protein molecules [32].

Covalent functionalization (chemical) includes forming chemical linkage over the defective carbon atoms either at the sidewall or at the open end caps (tips) of CNTs. Therefore it can also be known as defect functionalization [25]. Treatment with strong acids can be applied to functionalize CNTs by converting to sp^2 hybrid carbon atoms to sp^3 carbon atoms during oxidation process. As a result of exposure to strong

acids such as nitric acid, sulfuric acid or their mixture, oxygen containing functional groups such as carboxyl (-COOH), hydroxyl (-OH) and carbonyl (-C=O) groups anchor on the CNT surface (Figure 2.10). Obtained hydrophilic head groups will lead to CNT solubilization in most of the common polar solvent through their electrostatic repellency. These oxygenated groups lead to dramatically increase in reactivity of CNTs and evolution of their adhesion to the host polymer matrix. The functional groups on the sidewall allow further functionalization as well. Chemical functionalization prevent from reagglomeration of CNTs by offering long term stable dispersibility and miscibility. Although chemical functionalization has advantages, some physical and electrical properties of CNT can be impaired [30].

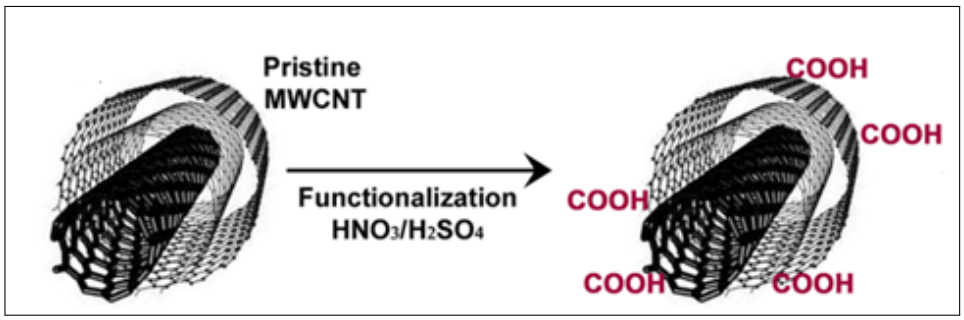

Figure 2.10 Schematic presentation of oxidation [33].

2.4 Methods for Nanocomposites Fabrication

A great number of approaches are come up with to manufacture CNT reinforced polymer nanocomposite which can vary depending on the type of polymer.

2.4.1 Solution Casting

Solvent casting method is one of the easiest way widely applied to fabricate CNT/polymer nanocomposite in the form of film. On the other hand, this simple processes is limited to polymers which are soluble in the common organic solvents. For solution mixing method, preparing suspension of CNT is necessary in the desired polymer solution via mechanical stirring or ultrasonic agitation which in turn alleviates

the dispersion of nanotubes. Followed by the homogeneous suspension, the solution is placed into mold and the solvent is allowed to evaporate during drying stage of process to form the CNT/polymer film nanocomposite. However there is a limitation of this technique that owing to long evaporation time, CNT can tend to form bundles preventing nanotubes from homogeneous dispersion in the host polymer matrix. The solvent selection depend on the solubility of the polymer which is of importance in term of properties of resulted nanocomposite. The complete removal of solvent is also crucial [23].

2.4.2 Melt Mixing

The melt compounding method is compatible with the thermoplastic polymer/CNT nanocomposite and mostly applied on a commercial scale. This method is suitable polymers of which ability to dissolve is impossible. High magnitude of shear occurred throughout the melt mixing process makes possible CNT bundles exfoliate with simultaneous dispersion and distribution in the host polymer melt. The elevated temperatures is generally utilized to render polymer less viscous and generate high shear forces to disperse nanotube bundles. Twin screw extruder is used to produce a composite masterbatch then obtained substrate can be shaped differently by using injection molding or compression molding technique. This approach is viewed as not effective in dispersion of CNT into polymer matrix although it has advantages of simplicity and speed of process [23].

2.4.3 In-situ Polymerization

This method enables combining of CNT with a high molecular weight polymer chain. When it comes to insoluble and thermally unstable polymers, in-situ polymerization technique works for production of composites with higher CNT loading. This method also shows superiority over the other composite fabrication methods. In the growth stage of polymerization, getting intimate chemical affinity between CNTs and

polymer chain is easy that results in obtaining much stronger interface which is necessary for a good load transfer from matrix to nanotube. Grafting of large polymer molecules onto the side walls of CNT are carried out by polymerization of monomers in the presence of CNT. Using low viscosity of beginning polymer is beneficial In order to acquire a good distribution of CNT in composite as a result of a better infiltration into the CNT [23].

3. MATERIALS AND METHODS

3.1 Carboxyl functionalization of MWCNT

80 mg of pristine MWCNTs were treated with 40 ml of sulfuric acid (Sigma Aldrich, 95-98 %, H_2SO_4) and nitric acid (Sigma Aldrich, 65%, HNO_3) mixture with a volume ratio of 3:1, respectively. MWCNTs were subjected to continuous ultrasonic vibration in the H_2SO_4/HNO_3 solution mixture in an ultrasonic bath at 50°C for 24 hours. At the end of prescribed time of sonication, the suspension was diluted with 150 ml of deionized water to avoid damaging of the filter membrane. The resulting nanotubes-acid mixture was then vacuum filtered using a 0.2 μm polytetrafluoroethylene (PTFE) filter membrane. The resultant black solid of carboxylated-MWCNT (MWCNT-COOH) was collected on the filter membrane with repeated washing with deionized water until the pH was neutral. Finally, filter cake was dried at 60°C overnight. Figure 3.1 shows the oxidation reaction for this procedure:

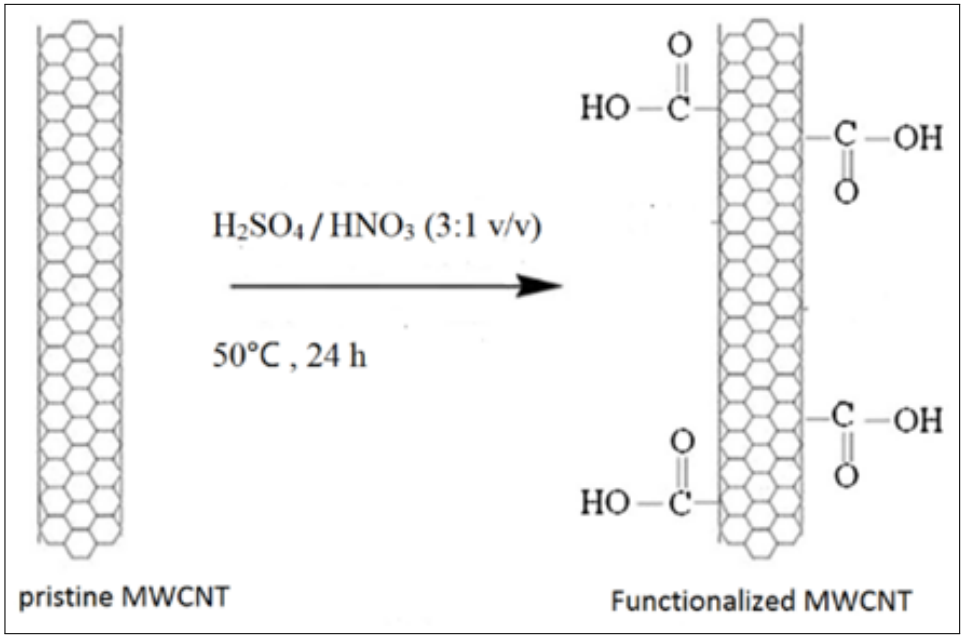

Figure 3.1 Representation of oxidation reaction [20].

3.2 Synthesis of sulfonated PEEK (SPEEK)

450G Victrex PEEK was kindly provided from Uniplast. Neat PEEK is a hydrophobic polymer and this prevents formation of its films by solution casting. PEEK is unable to dissolve in most of the solvents with the exception of high concentration of sulfuric acid. Sulfonated PEEK is hydrophilic which also enables its easy processability. Mechanical and thermal stability of the PEEK maintains thank to its aromatic backbone on which chemical modification through simple electrophilic substitution can be carried out by sulfonation. In order to sulfonate the neat PEEK, concentrated sulfuric acid (98% purity, Sigma Aldrich) was used as a sulfonating agent. The Figure 3.2 shows sulfonation reaction. The pure PEEK was added into concentrated sulfuric acid with a ratio of 8-10 wt. %. The solution mixture was heated up to 60 °C in a water bath for 24 h. Once PEEK was dissolved in the sulfuric acid, and the solution became viscous with a dark red color, sulfonated PEEK (SPEEK) was formed. After this, the polymer solution was stirred for another half an hour at 50°C. Sulfonation reaction, was terminated by gradually pouring over excess of ice cold deionized water under mechanical stirring and as a consequence the precipitated SPEEK turned to white color. The precipitate was kept in the ice cold water overnight and subsequently washed with distilled water by vacuum- filtering until pH was neutralized. Finally, samples were dried at 50°C for 24 hours. Figure 3.3 represents the experimental stages of sulfonation process.

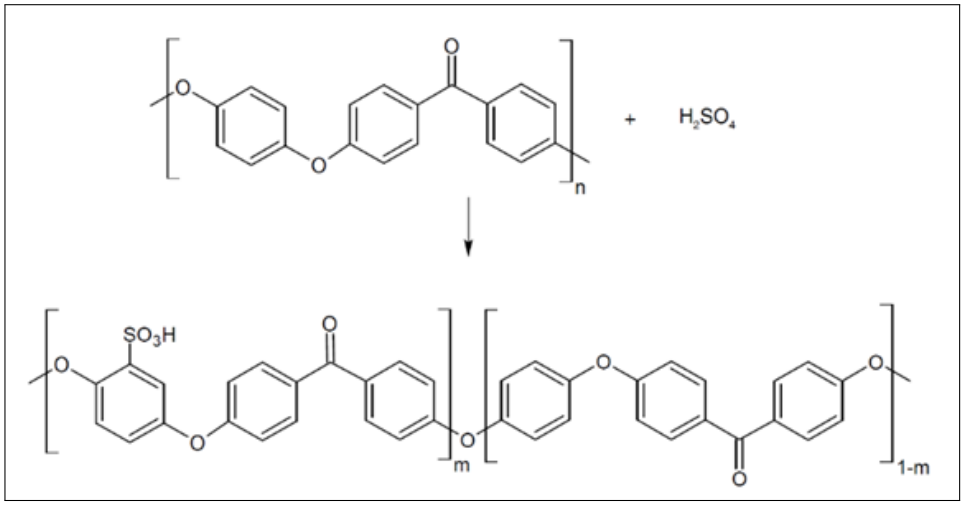

Figure 3.2 The reaction for the production of Sulfonated PEEK [34].

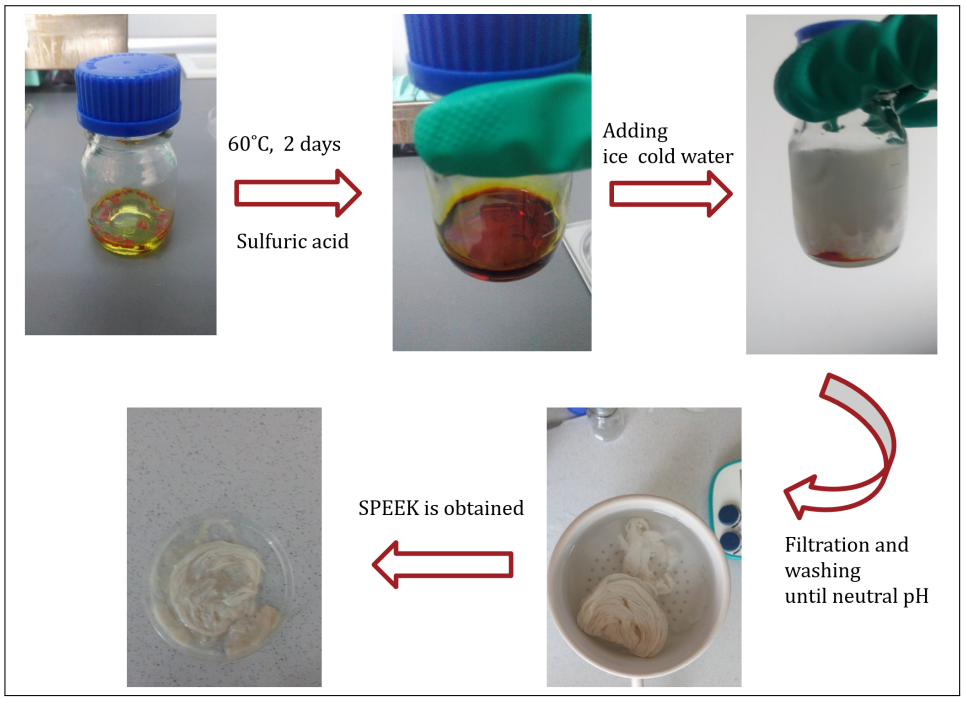

Figure 3.3 Experimental procedure of sulfonation reaction.

3.3 Fabrication of SPEEK/CNT Nanofilm

SPEEK was dissolved in 10 wt.% dimethylformamide (DMF). 0.5, 1 and 2 wt.% MWCNT, were incorporated into 10 wt.% SPEEK solution to produce carboxylated-MWCNT/ SPEEK nanocomposite films. In this process, 1g SPEEK was dissolved in 6 ml DMF using a mechanical stirrer. SPEEK solution was filtered with a 0.45 μm PTFE membrane. The Carboxylated-MWCNT was dispersed in 4 ml of DMF with an ultrasonicator (Bandelin) for about 2 hours. These two solutions were blended and magnetically stirred overnight to obtain a homogenous solution. Finally, before casting, blended solution was homogenized for an hour. Then films were casted and dried in an air oven at 60°C for 48 hours. After complete evaporation of the solvent nanocomposite films were peeled off with the addition of deionized water. Figure 3.4 displays hydrogen bonding formation emerged strong interfacial adhesion between SPEEK and f-CNT. Figure 3.5 illustrates the resultant SPEEK film and SPEEK/CNT nanofilms.

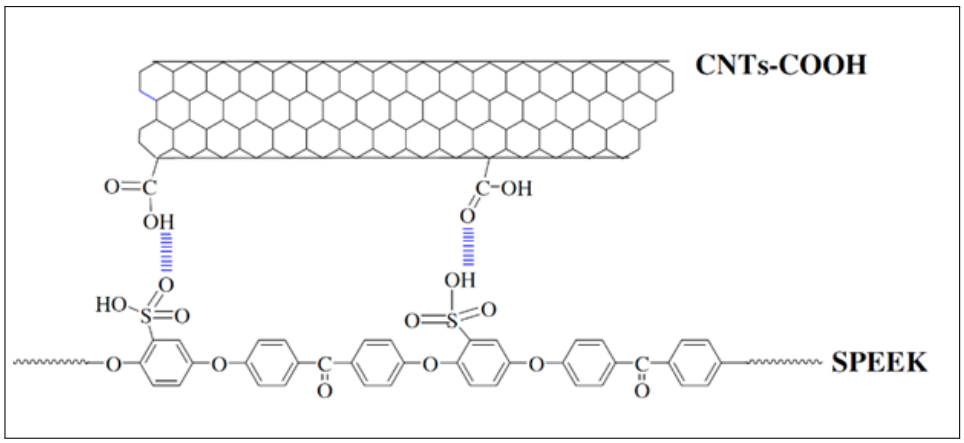

Figure 3.4 Formation of hydrogen bond between -COOH group of functionalized CNT and $-SO_3H$ sulfur group of SPEEK [35].

The miscibility of this components become easier through hydrogen linkages between the hydrophilic functional groups. Table 3.1 gives experimental groups for investigation effect of f-CNT addition into SPEEK polymer matrix on mechanical properties, surface morphology and biocompatibility in the produced nano-films compared to pure SPEEK.

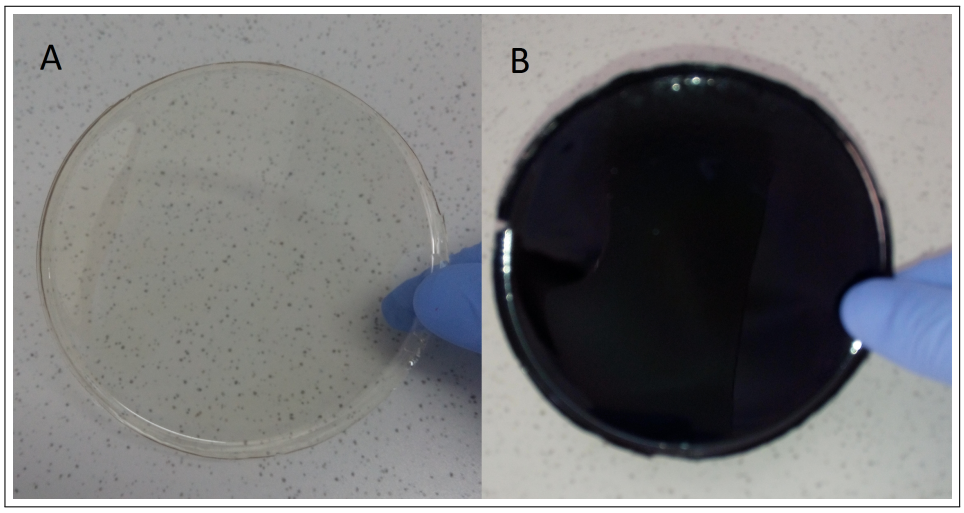

Figure 3.5 Obtained SPEEK film (A) and SPEEK /CNT nanofilm (B).

Table 3.1
SPEEK/CNT composite concentration and their designations.

Designations	SPEEK content (gr)	CNT content (gr)	Concentration (CNT/SPEEK)
SPEEK/CNT 0.5	1	0.005	0.5 wt/wt %
SPEEK/CNT 1	1	0.01	1 wt/wt %
SPEEK/CNT 2	1	0.02	2 wt/wt %

3.4 Aminolysis: Preparation of SPEEK/MWCNT-NH_2 Nanofilms

The nanocomposite films with a size of 1x2 cm^2 were immersed in 25, 50 and 75 v/v % diluted 400 μl hydrazine monohydrate solution. Pre-determined reaction times (15, 30 and 45 min) were also performed for each concentration of solution at room temperature to come up with the optimal concentration and reaction time to aminolyze the surface of SPEEK/MWCNT nanofilms. When aminolyzation reaction was terminated for every given time, resultant samples (SPEEK/MWCNT-NH_2) were thoroughly rinsed with ultra-purified deionized water for several times with deionized water in 15 min intervals to eliminate the unreacted hydrazine. Finally samples were dried at 30°C for overnight. Figure 3.6 exhibits that how the hydrazine molecule interacts with the ketone groups existing in the polymer backbone.

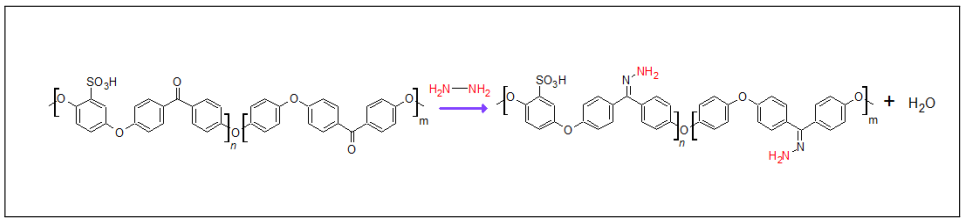

Figure 3.6 Formation of NH_2 groups on SPEEK (drawn in ACD/Chem Sketch freeware, ACDLABS 2016.2).

Figure 3.7 represents the free NH_2 groups on nanofilms surface which provides for further modification.

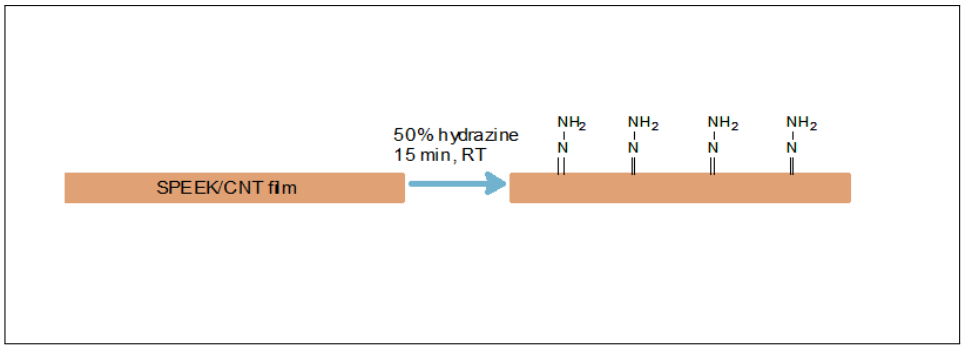

Figure 3.7 The schematic representation of aminolysis (drawn in ACD/Chem Sketch freeware, ACDLABS 2016.2).

3.5 Surface Modification of Nanofilms with L- Arginine

The amino acid molecules were covalently grafted on the nanofilm surface. In order to avoid protein aggregation, modification was governed in two steps. Firstly, aminolyzed nanofilms were incubated in 1 wt. % glutaraldehyde (GA) solution at pH 7.0 for 3h at room temperature. The reaction occurs between the free NH_2 groups and aldehyde group of GA and -N=CH- linkages are formed by yielding one free aldehyde group for further modification as well as. Then samples were washed with a large amount of deionized water to remove the unreacted GA. Then, nanofilms were immersed into PBS with 2 wt. % L-arginine for 24 h at room temperature. After incubation period, nanofilms were rinsed thoroughly with large quantity of deionized water for 2 hours at an interval of 15 min. L-arginine modified nanofilms (denoted

SPEEK/CNT-L-arg) were accomplished with the chemical reaction between the free aldehyde groups of GA and the amino groups of L-arg via imine bond (-C=N-) formation. Figure 3.8 shows the reaction carried out [15].

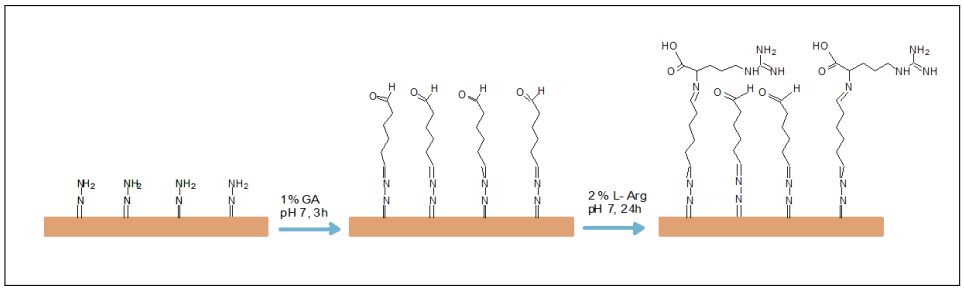

Figure 3.8 The schematic representation of SPEEK/CNT nanofilm modification with L-arginine (drawn in ACD/Chem Sketch freeware, ACDLABS 2016.2).

3.6 Surface Characterization of the Nanocomposite Film

The characterization of the nanocomposite films was performed in three distinct categories:

- Chemical Characterization (H-NMR, XPS and FT-IR, water contact angle measurements (WCA))
- Morphological characterization (AFM)
- Mechanical characterization (DMA)
- In vitro biological characterization (Alamar Blue)

3.6.1 Fourier Transform Infrared (FTIR) Spectroscopy Analysis

FTIR spectra of nanocomposite film samples were recorded on Thermo Scientific Nicolet 380 FT-IR spectrometer in a transmission mode to identify the chemical structure of PEEK and SPEEK. FTIR spectra was also conducted for determination of the carboxyl functionalization onto MWCNT through acid oxidation. The measurement

of FTIR spectra were taken within the range of 500-4000 cm^{-1}. The FTIR analysis was performed at Boğaziçi University Chemistry Department.

3.6.2 Contact Angle Measurement

The hydrophobic or hydrophilic characteristic of plain and modified nanofilm surfaces were assessed via contact angle measurement. Static water contact angle of the unmodified and modified nanofilms were measured by sessile drop method using a Contact Angle Measurement Goniometer (CAM 101 KSV instruments) at Boğaziçi University Chemistry Department with about 3-5 μl deionized water droplets at ambient temperature. The image of droplet fall onto nanofilm surface was recorded within 20 second with 1 second time interval with a digital camera after introduction of water droplet onto film surface and the state of droplet at 30th second was taken into consideration to measure the water contact angle. For each experimental group five droplets were measured from different points of nanofilms surface and the result was presented as average of these ten values with standard deviation.

3.6.3 Proton Nuclear Magnetic Resonance (H-NMR) spectroscopy

Sulfonation is an electrophilic aromatic substitution of hydrogen atoms with sulfonate groups through monosubstitution reaction on benzene ring connected with two ether (-O-) bonds in the repeated PEEK unit [36]. Proton Nuclear Magnetic Resonance (H-NMR) spectroscopy was employed to identify the incorporation of the sulfonate group into the SPEEK structure by elucidating position of aromatic protons in hydroquinone ring. The degree of sulfonation of polymers was determined by calculating the ratio between related peaks. The spectra of the specimens were obtained in dimethyl sulfoxide-d_6 (DMSO-d_6) solution (3-5 wt. %). NMR data were acquired for 32 scans at room temperature. H-NMR spectra of all unmodified composites were recorded by using a Varian Mercury-VX 400 MHz BB at Boğaziçi University Advanced Technologies Research and Development Center.

3.6.4 X-Ray Photoelectron Spectroscopy (XPS) Analysis

The variation in the surface chemistry and valence (electronic) state of element existed over surface were observed before and after L-arginine immobilization. Elemental composition and chemical station of SPEEK/CNT, SPEEK/CNT-NH_2 and SPEEK/CNT-L-arg nanofilm surface was elucidated by using Thermo Scientific K-alpha X-ray Photoelectron spectrometer equipped with a monochromatized Al $K\alpha$ X-ray radiation ($h\nu$ = 1486.6 eV) as an excitation light source, operating at power of 72W energy, spot size of X-ray 400 μm and 90° angle. Performed XPS measurement for the survey spectra and high resolution spectra on the regions of interest were acquired at an electron pass energy of 150 eV and 50 eV, respectively. The data spectrum were curve-fitted using Gaussian-Lorentzian function in order to find peaks of different coordinated elemental components [37]. The signal of N1s core-level can be evaluated as an indicator of the immobilized L-arginine. The binding energies of C1s and N1s core levels were obtained then these peaks were deconvoluted into distinct components. Atomic percentages for C, O and N atoms on the surface were calculated. The analysis was carried out at Boğaziçi University Advanced Technologies Research and Development Center.

3.6.5 Force Microscope (AFM)

The surface roughness (Ra) values of the fabricated nanofilms and modified nanofilm were measured by using AFM (Ez-AFM nano-magnetics) in the contact mode at Istanbul Technical University, Physic Department in Nano-mechanic Lab. Observation surface topography and morphology was also carried out by AFM. The dimension of the scanning fields of samples were ranging from 5x5 μm to 20x20 μm acquired at fixed resolution (256x256 data points). The captured images from AFM were analyzed with Image Analyzer v1.4 processing software. CNT distribution in polymer matrix was investigated and the effect of CNT addition on morphology of the nanofilm surface was also assessed with AFM 3D images.

3.6.6 Dynamic Mechanical Analysis (DMA)

The temperature dependent mechanical and thermal properties of produced samples of nanocomposite films were analyzed by employing DMA Q800 Dynamic Mechanical Analyzer (TA Instruments) at Istanbul Technical University, Civil Eng. Faculty, in Experimental Mech. Lab. Data were obtained at a fixed frequency of 0.5 Hz with 0.01N preload force and $10\mu m$ oscillation amplitude. Measurement was governed in the linear viscoelastic region. Before starting to experiment, samples were heated up to 60°C then keep 30 min and it was waited for cooling up to 35°C itself. The storage modulus and glass transition temperature of the samples were determined with the temperature variant, at a heating rate of 3°C/min, from 25°C to 190°C. The analyzed samples had an approximate size of 13 x 5 x 0.15 mm^3.

3.7 Cell Culture Studies

To evaluate the effect of CNT addition and L-arg modification on the cell viability and morphology, cell culture studies was carried out with human fetal osteoblast (hFOB 1.19, ATCC) cells. The cells were cultured in the Dulbecco's Modified Eagle's Medium (DMEM)/Nutrient Mixture F-12 DMEM/F-12 (Sigma) medium supplemented with 10% (v/v) fetal bovine serum (FBS), 12.5% (v/v) glutamine and 1% (v/v) penicillin/streptomycin.

3.7.1 In vitro hFOB Culture

SPEEK, SPEEK/CNT 2 and SPEEK/CNT-L-arg study groups were cut into circular discs with 9 mm diameter. Then the samples were sterilized by exposure to UV radiation for 1 hour per side. Sterile nanofilms were placed into 48 well-plates and the cells was seeded on the modified and unmodified films with a density approximately of 1.5 x10^4 hFOB. The cell culture which included the cell-seeded nanofilms were sustained in the incubator at 37°C and 5% CO_2 and 95% humidified air.

3.7.2 Alamar Blue Assay

Alamar Blue (AB) assay was performed to explore the cell viability quantitatively for SPEEK, SPEEK/CNT2, and SPEEK/CNT L-Arg study groups. AB dye leads to higher intensity readings on the spectroscopy at a 570 nm redox reaction due to metabolic activity of the cell [38]. The AB test was applied the culture after incubation at 1^{st} and 3^{rd} days. The sample number was five (n=4) for each study group and medium without cells was used as a negative control group. On the test day, the old medium was decanted and 200 μm fresh medium was added in to every single well and supplemented with 10% of culture medium and subsequently Alamar blue (20 μm) was added. Finally, the 48 well tissue culture plates were incubated further 3.5 hours at 37°C environment. After incubation, the culture of 100 μm solution was taken and transported into 96 well tissue culture plates to measure the reduction of Alamar blue dye at 570 and 595 nm wavelength by via a microplate reader (BIO-RAD Mark, Microplate Reader). The equation 3.1 was used to determine the percentage of reduction of Alamar Blue (AB).

$$\%Reduced = \frac{(\epsilon_{OX}).\lambda_2.A\lambda_1 - (\epsilon_{OX}).\lambda_1.A\lambda_2}{(\epsilon_{red}).\lambda_1.A'\lambda_2 - (\epsilon_{red}).\lambda_1.A'\lambda_2} \tag{3.1}$$

where,

ϵ_{OX}= molar extinction coefficient of AB oxidized form

ϵ_{red}= molar extinction coefficient of AB reduced form

A= absorbance of test wells at 570 and 595nm

A'= absorbance of negative control well at 570 and 595nm

λ_1= 570 nm

λ_2= 595 nm

4. RESULTS

4.1 Fourier Transform Infrared Spectroscopy (FTIR) Analysis of f-MWCNT

The spectra for FTIR measurements of MWCNT, f-MWCNT and commercial cheap tube MWCNT were presented in the Figure 4.1.

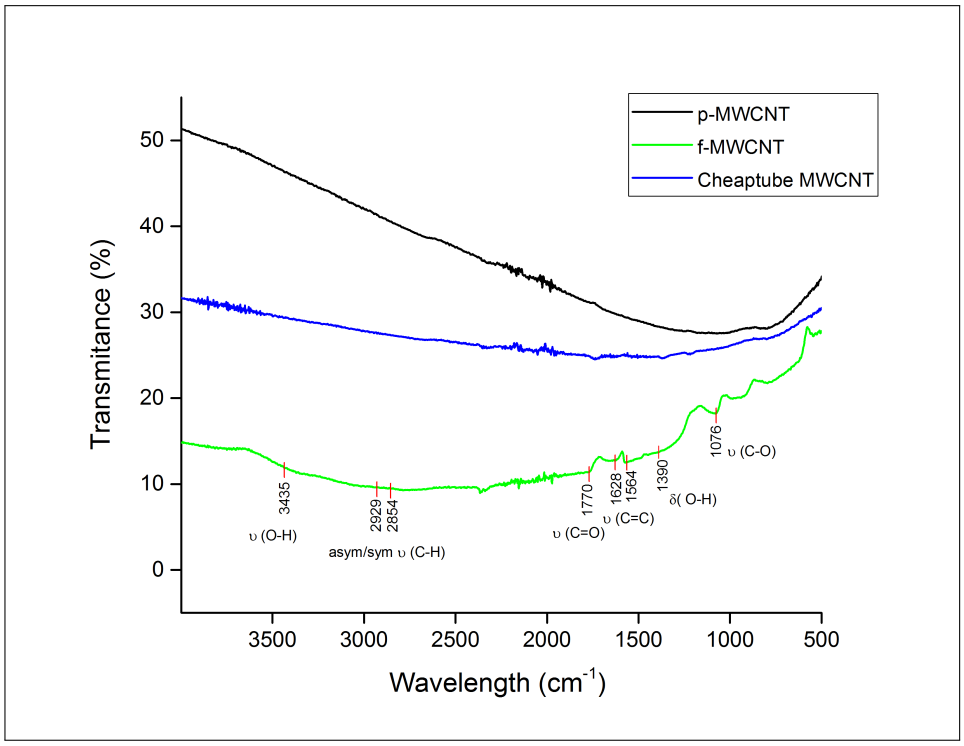

Figure 4.1 FTIR spectra of MWCNT, f- MWCNT and commercial cheaptube carboxyl functionalized MWCNT.

The absorption band at 3435 cm^{-1} was associated with the stretching vibration of hydroxyl group (-OH) bonds in the -COOH groups. The absorption peaks observed at 2929 cm^{-1} and 2854 cm^{-1} were correlated with the asymmetric and symmetric stretching vibration of (O-H) binds in the terminal carboxyl groups attached to MWCNT surface and sidewalls [39]. The emergence of the additional peaks at 1770 cm^{-1} resulted from the carbonyl group in -COOH [40, 41]. Observed peak of C=C bonds appeared at wavelengths of cm^{-1} and 1564 cm^{-1} [42, 43, 39, 44, 45]. The

bands at 1390 cm^{-1} and 1076 cm^{-1} was attributed to O-H bending and C-O stretching vibration in carboxyl groups formed by acid functionalization, respectively [44]. The evidences illustrated the successfulness of the incorporation of carboxyl included groups on sidewalls and ends of MWCNT upon oxidation.

4.2 Sulfonation of PEEK

4.2.1 Fourier Transform Infrared Spectroscopy (FTIR) Analysis

The successful substitution of sulfonic acid group on PEEK structure was proved through the comparison of FT-IR spectra of SPEEK with that of PEEK in the Figure 4.2.

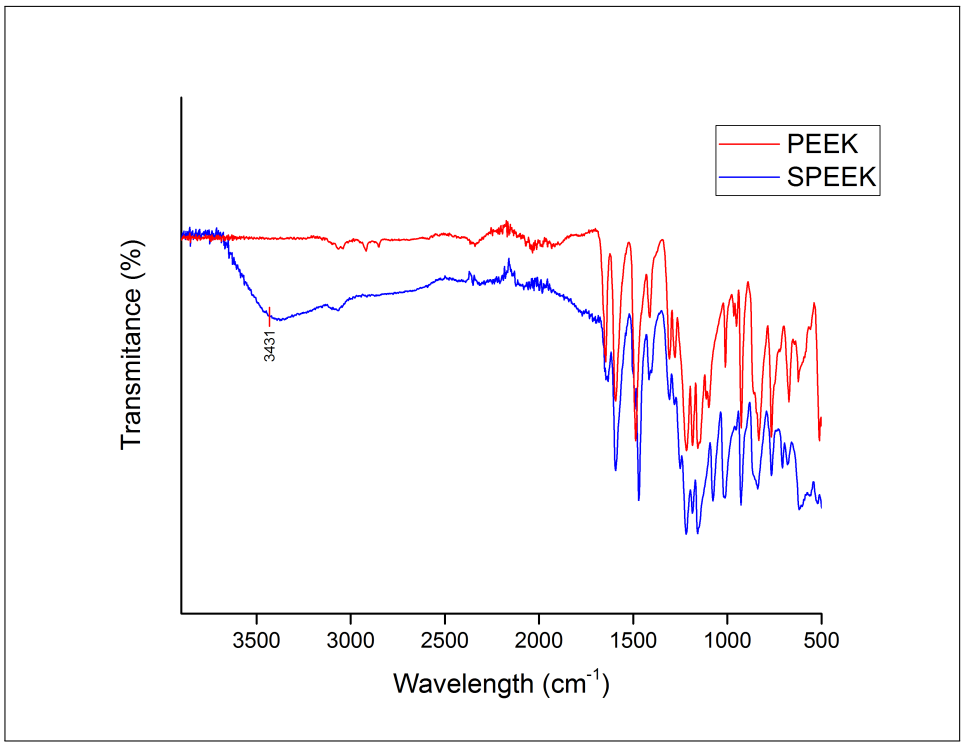

Figure 4.2 FT-IR spectra of SPEEK and PEEK.

Observation of the peak in the Figure x the spectrum of SPEEK shows the broad band at 3431cm^{-1} were attributed to the O-H stretching of SO_3H and absorbed water moisture.

Figure 4.3 demonstrates the magnified spectra of PEEK and SPEEK FTIR measurements to be enable to observe the shifts at a certain interval.

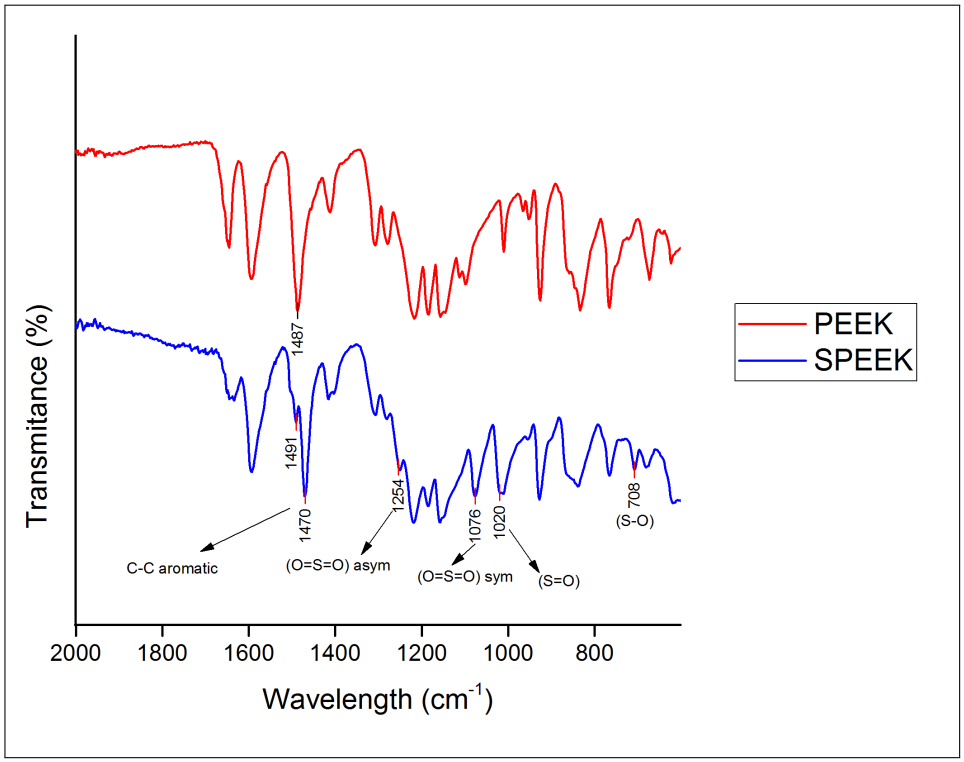

Figure 4.3 FT-IR Spectra of SPEEK and PEEK within the range of 2000-800 cm^{-1} wavelength.

For the more detailed investigation spectra of SPEEK and PEEK was presented in the range of 2000-800 cm^{-1} in the Figure y. The band at 1487 cm^{-1} corresponding aromatic C-C ring in the PEEK was split into two additional characteristic peaks between 1470 cm^{-1} and 1491 cm^{-1}, which were associated with S=O, sulfonic acid group in SPEEK. The new absorption band in SPEEK spectra emerged at 1020 cm^{-1} and 1076 cm^{-1} were attributed to the S=O stretching and symmetric stretching vibration of the O=S=O, respectively. The peak absorption was observed at 1254 cm^{-1} which is assigned to the asymmetric stretching of O=S=O [46, 47, 48, 49]. Therefore, the results proved the presence of sulfonation of PEEK aromatic backbone.

4.2.2 Proton Nuclear Magnetic Resonance (H-NMR) Analysis

H-NMR was applied to investigate the structure and composition of SPEEK. Monosubstitution due to sulfuric acid reaction with PEEK was assessed by H-NMR spectrum. Figure 4.5 shows a distinct peak which is denoted as HE for the proton in ortho position of SO_3H and density of this single signal is associated with the content of SO_3H groups in the structure [36]. The peak at 7.24 ppm in the spectrum stand for the H_C protons in unsubstituted hydroquinone ring of repeated unit of PEEK. This H_C protons is differentiated into three categories H'_C, H'_D and H'_E. Introduced sulfonic groups into the hydroquinone ring gave rise to a significant downfield shift of the H'_C, H'_D, and H'_E signals in the hydroquinone ring at 7.21 ppm, 7.09 ppm, and 7.50 ppm, respectively. The degree of sulfonation (DS) of SPEEK was quantitated from spectra of H-NMR by calculating the ratio of peak area of the distinct $H'_E(A_{HE'})$ signal to the peak area of all the other aromatic hydrogens corresponding with $H_A, H_{A'}, H_B, H_{B'}, H_C, H_D signals(AH_{A,A',B,B',C,D})$. The nomenclature for displaying presence of the characteristic protons in the aromatic ring in the sulfonated PEEK repeat unit is described as shown in the Figure 4.4 [50].

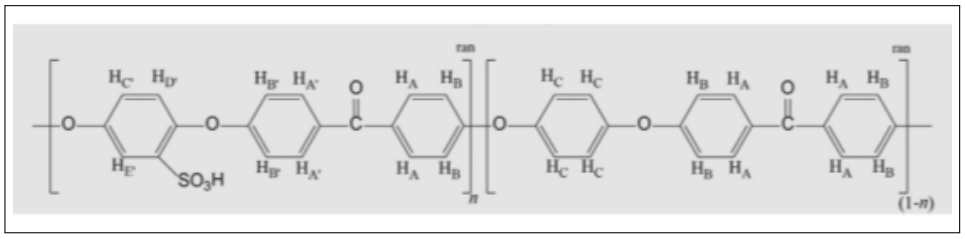

Figure 4.4 Nomenclature of the aromatic protons of PEEK and SPEEK repeat unit [51].

This HC protons is differentiated into three categories: HC', HD' and HE' which indicates the presence of protons of the -SO3H groups as shown in Fig, while the sulfonic group is attached to the aromatic ring of PEEK. The DS (degree of sulfonation) was determined through integration of distinct aromatic signals [52, 53]. DS was calculated using equations 4.1 and 4.2 [54]:

$$\frac{n}{12-2n} = \frac{A_{H_E}}{\sum A_{H_{A,A',B,B',C,D}}} \tag{4.1}$$

where 'n' is the number of HE per repeat unit.

$$DS(\%) = n \times 100 \qquad (0 < DS < 1) \tag{4.2}$$

The estimated degree of sulfonation of the prepared SPEEK in this study was calculated as approximately 81%.

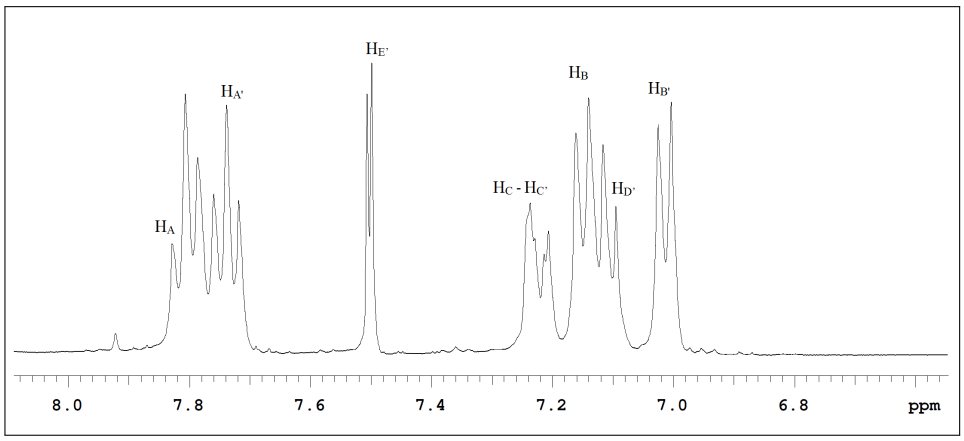

Figure 4.5 H-NMR spectrum of SPEEK in DMSO-d.

4.3 Water Contact Angle Measurements

In order to investigate the effect of additional CNT and modification with L-arginine on hydrophilicity of the SPEEK and SPEEK/CNT nanofilms, water contact angle measurement was conducted. Figure 4.6 demonstrates that SPEEK and SPEEK /CNT nanofilms had lower contact angles than pure PEEK which suggested that the nanocomposite films were more hydrophilic. The average values of water contact angle with standard deviation among nanocomposite films with different concentrations of

CNT were 67.77±6.5, 60.33±4.1, 56.57±7.4 and 50.82±6.5 for SPEEK, SPEEK/CNT 0.5, SPEEK/CNT 1 and SPEEK/CNT 2, respectively. There is a slight decrease with the increase of wt. % of CNT. The hydrophilicity of SPEEK and its composite with different concentration of CNT is better than the untreated PEEK which was 103.5°C. But the effect of CNT on the wettability was insignificant due to embedding of CNT into matrix.

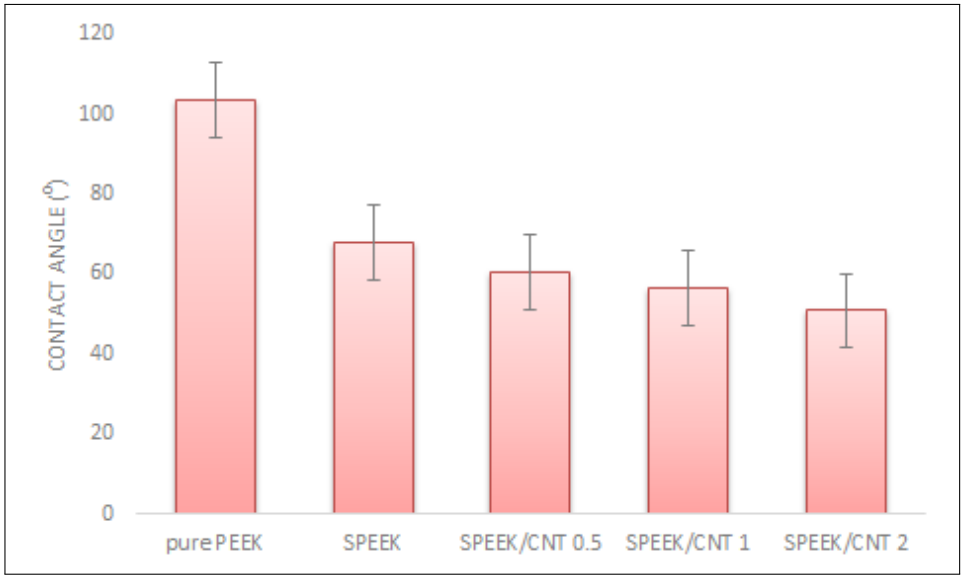

Figure 4.6 Surface Contact angles of PEEK granule, SPEEK membranes and SPEEK/CNT nanofilms.

Figure 4.6 exhibits the captured images of nanocomposite films for 20^{th} second of water droplet on the surface.

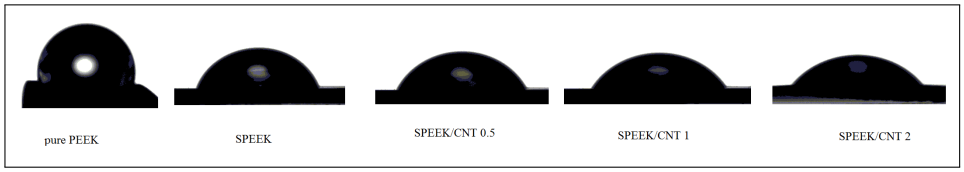

Figure 4.7 Image of nanofilms for contact angle measurement.

Once the nanofilms were immobilized with L-arginine amino acid the contact angle value did not exhibit a dramatic changes. The Figure 4.8 indicated the contact angle of L-arg modified nanofilm which was 56°.

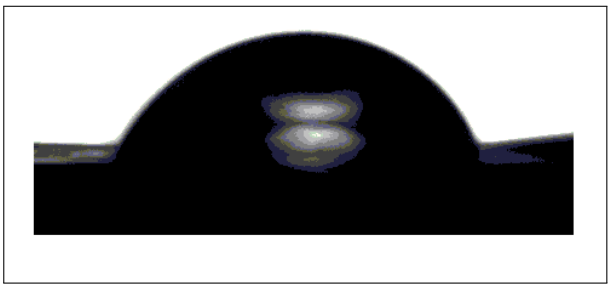

Figure 4.8 Image of L-arg modified nanofilm for contact angle measurement.

4.4 X-Ray Photoelectron Spectroscopy (XPS) Analysis

XPS analysis was used as a surface sensitive and nondestructive spectrophotometer technique. The electronic state of the surface and the chemical components detected owing to amino acid attachment over nanocomposite films surface were elucidated through this method [55]. XPS measurements were acquired for modified and unmodified SPEEK/CNT nanofilms in order to confirm the grafting of L-arginine onto SPEEK/CNT nanofilms surface. The survey scan spectra of SPEEK/CNT, SPEEK/CNT-NH_2 and SPEEK/CNT-L-arg nanofilms were collected to demonstrate the L-arginine attachment on the surface of SPEEK/CNT nanofilm. The Figure 4.9 displayed survey spectra of samples included essential peaks that there are three main elemental species such as C, O and N. Respective photoelectron peaks corresponding to C1s and O1s appeared at binding energy 285 and 532 eV for all type of nanocomposite films. However, the photoemission peak existing at 400 eV was only present for SPEEK/CNT-NH_2 and SPEEK/CNT-L-arg nanocomposite films, which confirms the presence of N1s atomic component. Moreover, Figure 4.10 shows that after immobilization of L-arg, the intensity of N1s peak significantly increased with the increased N composition which indicated successful immobilization of L-arg.

The atomic percentage concentrations of carbon, oxygen and nitrogen atoms were also measured by integrating peak areas of the C1s, N1s, and O1s from the XPS survey spectra. The overall nitrogen content in the nanofilms were determined by using the ratio N1s to C1s integrated peak areas for before and after L-arginine immobilization. Table 4.1 revealed that Carbon (C), Oxygen (O) and Nitrogen (N)

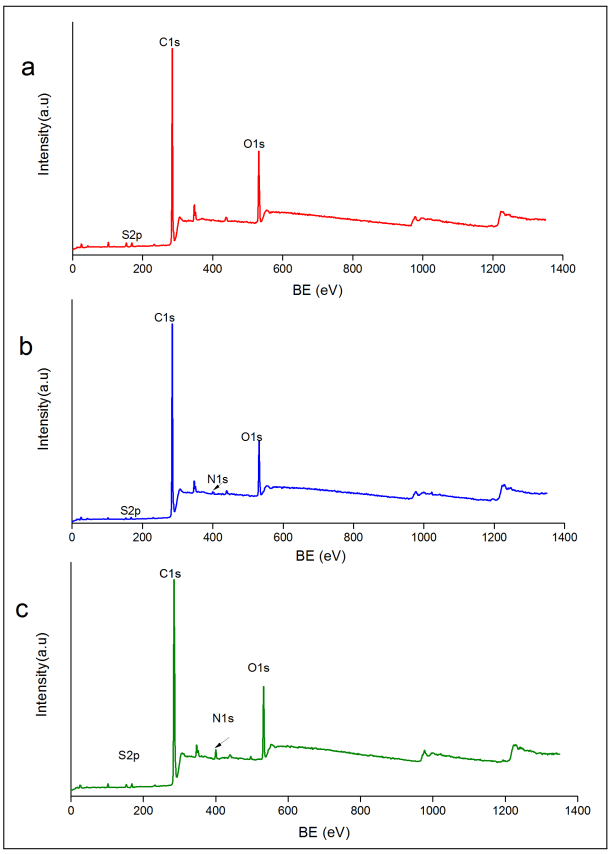

Figure 4.9 Comparison of nanofilms XPS survey spectrum of surface a) Survey scans of SPEEK/CNT, b) survey scan of SPEEK/CNT-NH_2, c) survey scan of SPEEK/CNT-L-arg nanofilm.

atomic concentration for all experimental groups and the measured nitrogen/carbon (N/C) ratio on the nanofilm surface which is higher on the L-arg modified nanofilm than on that of hydrazine treated counterparts. According to XPS data, the nitrogen atomic concentrations on SPEEK/MWCNT-NH_2 and SPEEK/MWCNT-Arg increased by 1.13% and 3.12%, respectively. In addition, a higher N/C ratio was determined on the surface of SPEEK/MWCNT -Arg (0.033) than on that of SPEEK/MWCNT-NH_2 (0.013).

XPS is also able to determine variance in bonding environments of individual elements material with curve-fitting of the element's photoemission peak [56]. The chemical bonding state of elements presenting on the surface was tried to deduce from the shape and shift of the XPS spectra. Further information was obtained from investigation of C1s and N1s high resolution spectra with fittings curves for before and after immobilization of L-arg. In order to identify the different bonding states of C atoms,

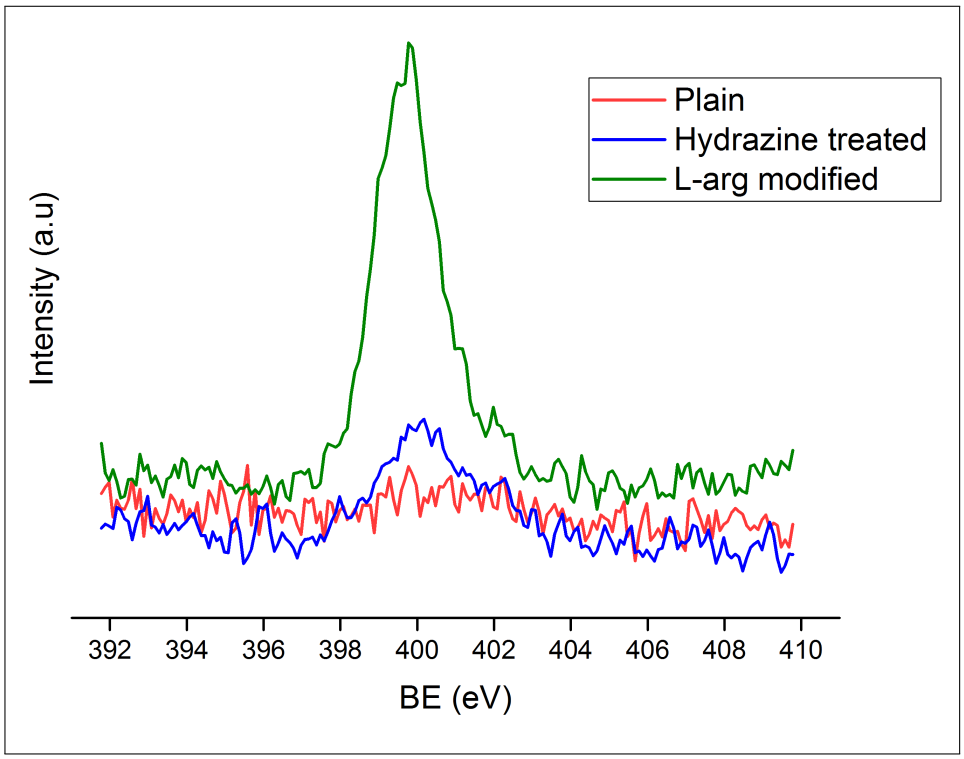

Figure 4.10 Increase in the signal of the N1 envelope (core level) spectra of nanocomposite films.

Table 4.1
Surface elemental composition of modified and unmodified SPEEK/CNT films.

Sample	Elemental atomic concentration (%)			Ratio
	C1s	O1s	N1s	N/C
SPEEK/CNT	80.77	13.3	0	0
SPEEK/CNT-NH_2	83.97	11.15	1.13	0.013
SPEEK/CNT-Arg	79.59	12.82	3.12	0.039

high resolution of C1s spectra were deconvoluted into three components as shown in the Figure 4.11.

The characteristic photoelectron peaks emerged at binding energies of 284.44, 285.64 and 288.24 eV for hydrazine treated nanofilm composite and at that of 284.57, 285.78 and 288.15 eV for L-arg modified nanofilm composite. The characteristic photoemission peaks, observed at 284.44, 285.64, and 288.88 eV, were attributed to the

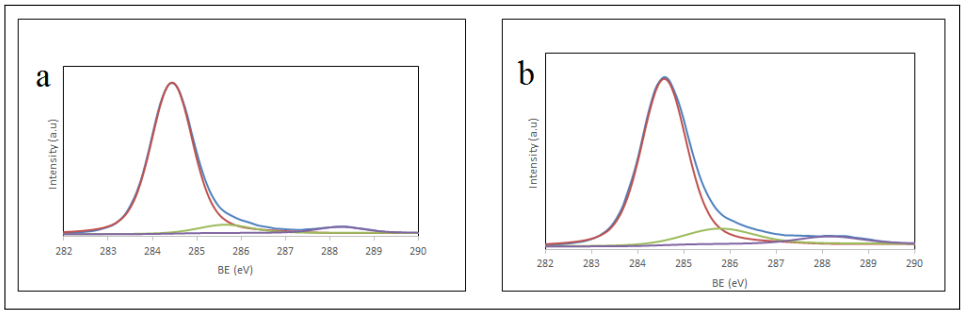

Figure 4.11 C1s high resolution of a) hydrazine treated nanofilm and b) L-arg modified nanofilm.

C-C/C=C, C-O/C= O, and C=N bonds, respectively [57]. After grafting of L-arginine there is slight shift in binding energies. The new peak of C-N of which binding energy is corresponded to 285,78 existed from - C-NH-C- on the nanofilm surface, which signs to be grafted of L-arg. However, it is not enough distinguishable peak to observe due to respective peaks may overlap in narrow (high resolution) range. Table 4.2 presents the chemical state of C element with corresponding binding energies, FWHM values and atomic concentration.

Table 4.2
Chemical Bonds and corresponding binding energies of C atom.

Nanofilm Designation	**Elements**	**Binding Energies (eV)**	**FWHM**	**Atomic Conc. (%)**	**Chemical state**
SPEEK/CNT-NH_2	C1s	284.44	1.11	89.66	C-C/C=C
		285.64	1.38	6.18	C-O/C= O
		288.24	1.26	4.16	C=N
SPEEK/CNT-L-arg	C1s	284.57	1.16	82.72	C-C/C=C
		285.78	1.79	11.98	C-O/C=O
		288.15	1.66	5.3	-C-NH-C-

The analysis for nitrogen region of the XPS spectra was also proved the deduction. The high-resolution N1s core level spectra for hydrazine treated and L-arg modified nanofilms were fitted with Gaussian curves (Figure 4.12).

N1s spectrum of SPEEK/CNT- NH_2 was deconvoluted into two characteristic

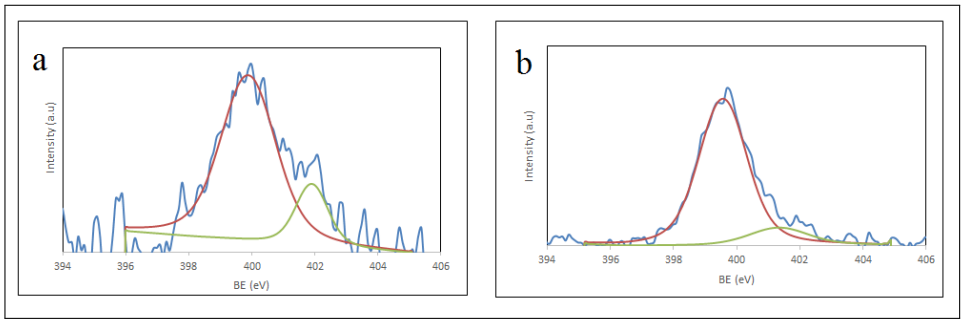

Figure 4.12 N1s high resolution of hydrazine treated nanofilm (a) and L-arg modified nanofilm.

peaks at which binding energies of N coordinated atoms are 399.88 and 401.9. The peak observed at 399.88 eV associated with free amino group (NH_2) and N=C [58]. That binding energy may also be attributed to azo bridges (-N=N-) in the hydrazine groups [59]. The second peak component appeared at 401.9 eV was assigned to N-H and ammonium groups (-NH_3^+) binding energies [60, 57]. The curve fitted spectra of SPEEK/CNT- L-arg was different which can suggest the appearance of L-arg on the nanofilm surface. The new peak component of N-C with N=C can be attributed to binding energy of 399.56 eV [61]. The binding energy of 401.33 may ascribed to C-NH-C bond [62]. Table 4.3 indicates the chemical state of N element with corresponding binding energies, FWHM values and atomic concentration.

Table 4.3
Chemical Bonds and corresponding binding energies of N atom.

Nanofilm Designation	**Elements**	**Binding Energies (eV)**	**FWHM**	**Atomic Conc. (%)**	**Chemical state**
SPEEK/CNT-NH_2	N1s	399.88	2.07	1	-N=N-, -NH_2, N=C
		401.90	1.22	0.22	N-H, $-NH_3^+$
SPEEK/CNT-L-arg	N1s	399.56	1.8	1	-N-C, N=C, -C=N-C-
		401.33	2.19	0.14	-C-NH-C-

4.5 Atomic Force Microscope

Surface roughness values of the fabricated and modified nanofilms are found with AFM. The alteration in the surface of nanofilms was also observed. The surface morphology and thickness profiles were presented at two different scanning size. In the Figure 4.13 demonstrates images scanned 5×5 micron field of nanofilms with thickness profile. The roughness of the films were 3.97 nm, 10.60 nm, 19.62 nm, 23.60 nm and 0.18 μm for SPEEK, SPEEK/CNT 0.5, SPEEK/CNT, SPEEK/CNT 2 and SPEEK/CNT-L-arg, respectively. It can be referred the effect of the CNT addition increases the surface roughness of the nanofilms. Moreover, CNT distribution within the polymer matrix was more homogenous in the polymer matrix and the surface for SPEEK/CNT 2 nanofilm in comparison with other groups. After L-arg immobilization through the nanofilm surface, the surface roughness were altered visibly at a micron scale. When compered 5×5 micron image of L-arg with 20×20 micron, There is no significant difference in the value of surface roughness which might mention that the L-arg was distributed equally all the surface. Pretty rougher surface of modified film may be evidence of the grafting of amino acid molecule. The Figure 4.14 additionally displays the 3D AFM images of nanofilms corresponding to 2D images in the Figure 4.13.

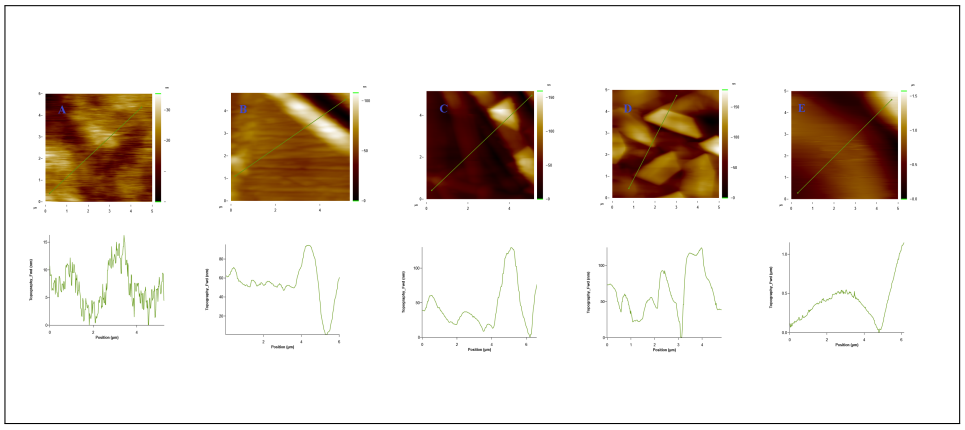

Figure 4.13 AFM 2D images with corresponding height (thickness) profile of SPEEK/CNT nanofilms at 5×5 micron A) SPEEK B) SPEEK/CNT 0.5 C) SPEEK/CNT 1 D) SPEEK/CNT 2 E) SPEEK/CNT-L-arg.

In the Figure 4.16 2D AFM images of nanofilms at 15×15 scanning scale were also showed. At size of 15×15 micron field, a single CNT particle was seen on the

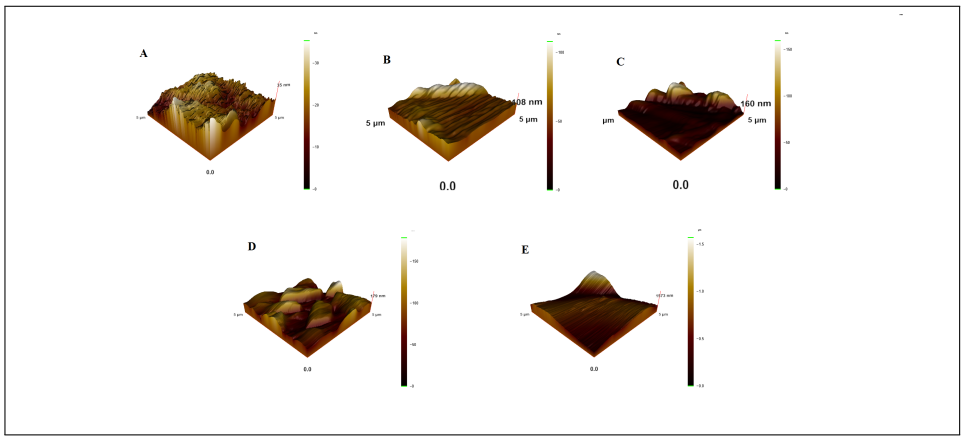

Figure 4.14 AFM 3D images of SPEEK/CNT nanofilms at 5×5 micron A) SPEEK B) SPEEK/CNT 0.5 C) SPEEK/CNT 1 D) SPEEK/CNT 2 E) SPEEK/CNT-L-arg.

SPEEK/CNT 0.5 nanofilm surface, which resulted in a considerable increase in the surface roughness for some zones. But the distribution of CNT was inhomogeneous. Surface roughness values for SPEEK/CNT 0.5, SPEEK/CNT 1, SPEEK/CNT 2 and SPEEK/CNT-L-arg were 136.61 nm, 18.12 nm, 36.43 nm and 0.22 μm, respectively. The roughness values were consistent only for SPEEK/CNT 1, SPEEK/CNT 2 and SPEEK/CNT-L-arg at a larger scale due to homogeneity. When it comes to SPEEK/ CNT 0.5 nanofilm it could not be said. Single CNT cylinder cause to increase roughness enormously resulting from nonhomogeneous distribution in polymer matrix. The Figure 4.15 gives the 3D AFM images of nanofilms corresponding to 2D images in Figure 4.16.

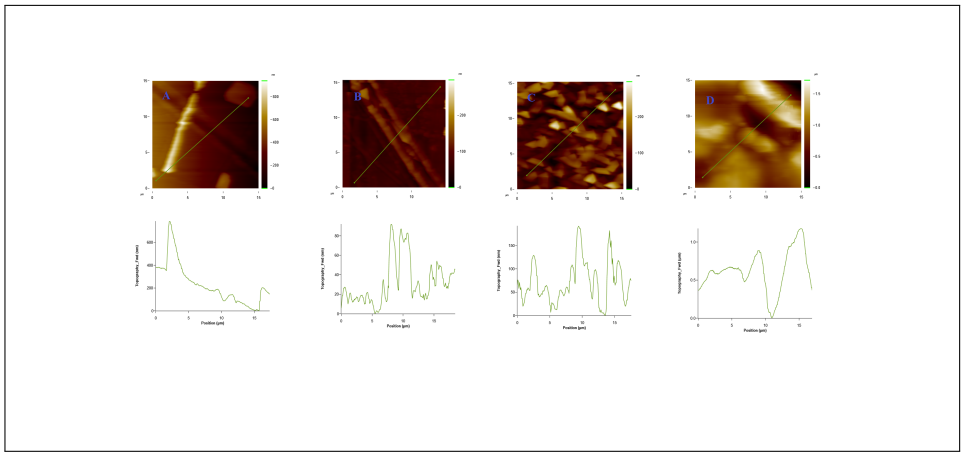

Figure 4.15 AFM 2D images with corresponding height (thickness) profile of SPEEK/CNT nanofilms at 15×15 micron A) SPEEK/CNT 0.5 B) SPEEK/CNT 1 C) SPEEK/CNT 2 D) SPEEK/CNT-L-arg.

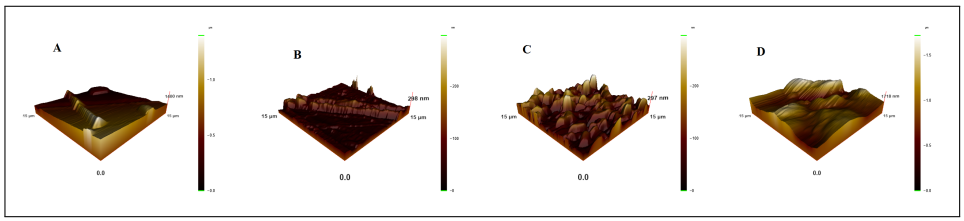

Figure 4.16 AFM 3D images and thickness profile of SPEEK/CNT nanofilms at 15×15 micron A) SPEEK/CNT 0.5 B) SPEEK/CNT 1 C) SPEEK/CNT 2 D) SPEEK/CNT-L-arg.

4.6 Dynamic Mechanical Analysis

The mechanical behavior of the nanofilms composites were influenced dramatically by carboxyl functionalized MWCNT addition. The mechanical properties of the film nanocomposite was strengthened with the incorporation MWCNT into SPEEK polymer matrix as a reinforcement agent. The curve for the storage modulus (E') of SPEEK/CNT nanofilms as the function of temperature were demonstrated in Figure 4.17.

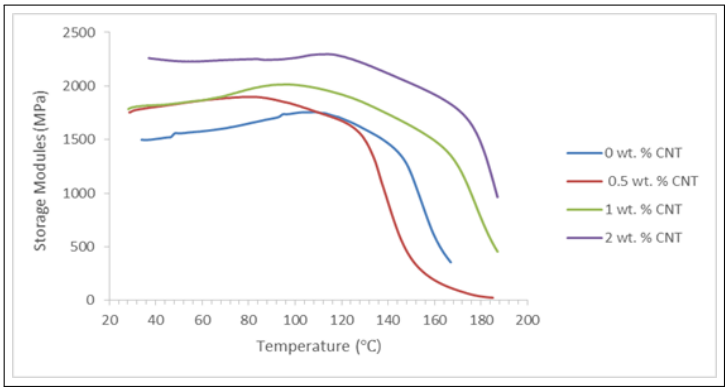

Figure 4.17 Storage modulus of SPEEK/CNT nanofilms.

The storage modulus represents the elastic behavior of polymer material. It should be equal to Young's modulus of material in ideal case [63]. Up to 100°C, the storage modulus of the samples were increasing slightly which might be due to removal of solvent stacked into nanocomposites during solvent casting which caused a plasticizing effect [64, 65]. The storage modulus values for SPEEK, SPEEK/CNT 0.5, SPEEK/CNT 1and SPEEK/CNT 2 were 1500 MPa, 1798 MPa, 1819 MPa and 2261 MPa at 37°C, respectively. There was an increment of storage modulus of nanocom-

posite films with the increasing wt. % of f- MWCNT. The enhancement of mechanical properties is related to formation of hydrogen bonds between hydrophilic functional groups of SPEEK and f-MWCNT which leads to a good interfacial adhesion resulted in a good load transfer from SPEEK as a polymer matrix to MWCNT [66]. Therefore the excellent mechanical strength of CNT owing to its pretty high elastic modulus can be totally transferred into polymer matrix by improving the modulus of the obtained nanocomposite films. Moreover, formation of hydrogen bonds constrains the slippage of polymer matrix chains in the structure [67]. In addition to hydrogen bonds, increase in homogenous distribution of f-MWCNT with increased f-MWCNT loading gives rise to elevated mechanical properties of resultant nanofilms as well [20].

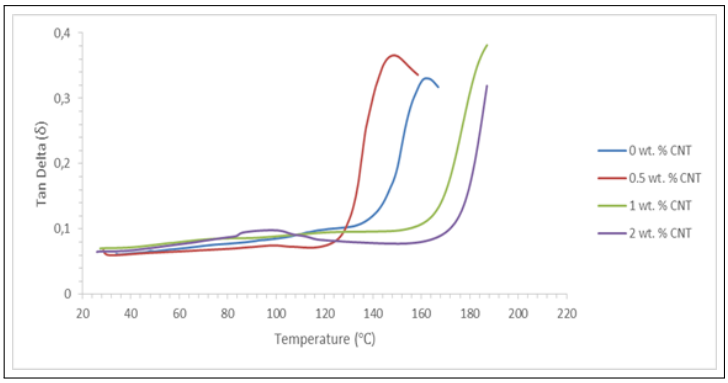

Figure 4.18 Tan delta of SPEEK/CNT nanofilms.

The curve in Figure 4.18 display variation of the phase angle ($tan\delta$) with the elevated temperature at a certain rate. It can be described as the ratio of loss modulus (associated with the viscos response of the polymer) to the storage modulus. The phase angle of material has sensitivity to its phase transition like glass transition of the polymer (Tg) [63]. Tg is the point where polymer side chain movement initiates. Therefore Tg is defined as the temperature at the peak or onset point in $tan\delta$ curves [68, 69, 64]. According to the Figure the Tg values of SPEEK film was 162°C at which the $tan\delta$ value was the highest. With the increased ratio of CNT in polymer matrix, the Tg values shifted from 162 to above 190°C. The reason why Tg was getting increased was the effect of nanoparticle stiffened. This effect hinder the polymer chain motion [68, 66]. However, as unexpected result that Tg of 0.5 wt. % CNT were less than the pure SPEEK.

4.7 Alamar Blue

Alamar blue is a non-cytotoxic redox indicator which elicit colorimetric change towards metabolic activity of the cells. It was governed to investigate cell viability on the modified and unmodified naonafilms. The equation 3.1 was used to calculate the percentage of reduced Alamar blue which correlated with the cell metabolic activity. The presented data was indicated as average with standard deviation and sample number was 4 for each study groups. Figure 4.19 showed the result of Alamar blue assay on day 1 after culturing of the cell seeded samples and the Alamar reduction percentage was 36.7 %, 38.7 %, 49.8 % and 66.9% for SPEEK, SPEEK/CNT 2 , SPEEK/CNT- L-arg and TCP, respectively. There was a significant increase in the cell viability for L-arg modified nanofilms which proved the favorable effect of L-arg on the cell proliferation.

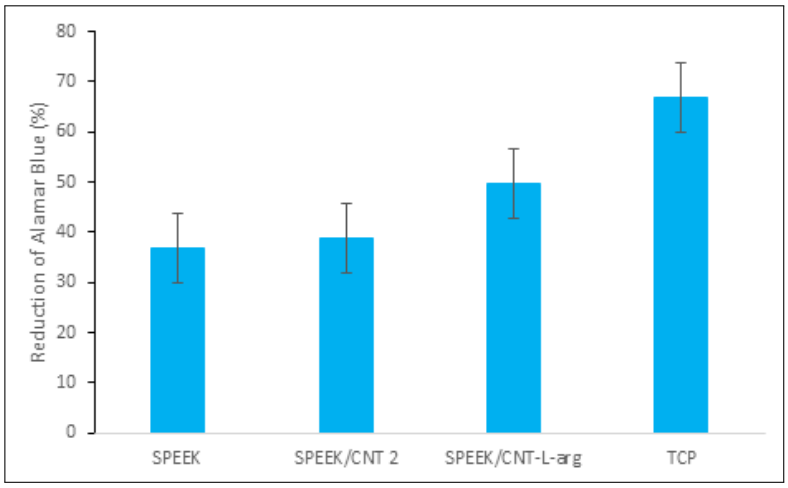

Figure 4.19 Alamar Blue assay result at first day (n=4).

Figure 4.20 demonstrated the 3rd day of cell culture on the samples and the percent of Alamar reduction was 184.8 %, 191.7 %, 272.7 % and 519.6 % for SPEEK, SPEEK/CNT 2, SPEEK/CNT- L-arg and TCP, respectively. Among the experimental groups, the highest cell proliferation was for the L-arg modified nanofilm study groups as well. For both days, when the Alamar blue assay was carried out, there was the same trend in the experimental group.

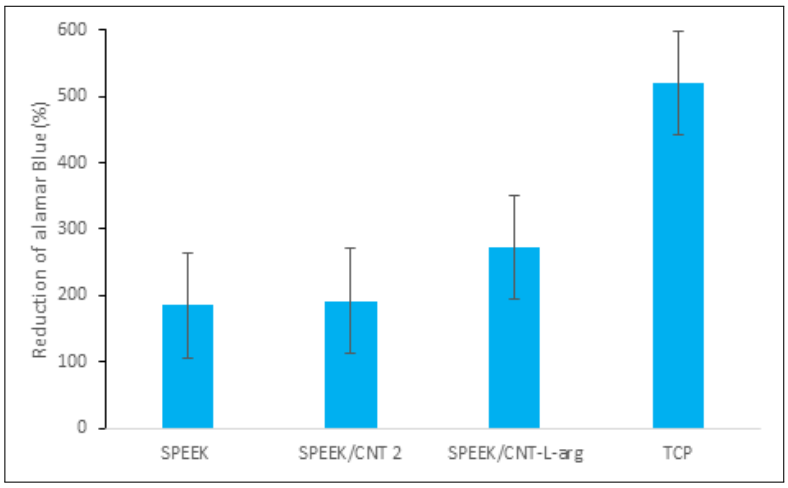

Figure 4.20 Alamar Blue assay result at third day (n=4).

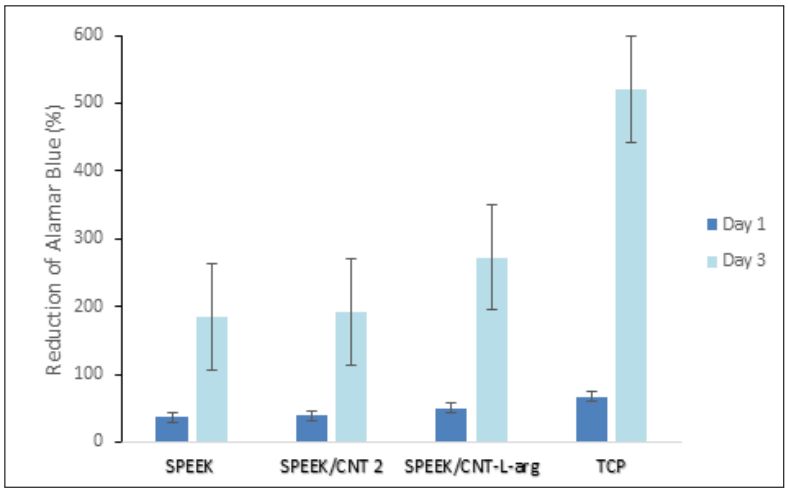

Figure 4.21 Comparison of first and third days' results of Alamar Blue assay.

Figure 4.21 displayed the comparison of 1st and 3rd day regarding with cell proliferation. Cell viability increased considerably while culturing is maintained from 1st to 3rd day.

5. DISCUSSION

PEEK is widely applied in medical field due to its biocompatibility, good wear resistance radiolucency and corrosion resistance which are of crucial value in load-bearing implant application. In addition, it is shows similarity to the bone in terms of biomechanical properties. Mechanical strength of PEEK can also be adjusted by the addition of some carbon based fillers. But, its bioinertness prevents well bone-implant integration. Some surface modification can be carried out to overcome unfavorable bioactivity of PEEK. To the end, L-arginine as a biomolecule functionalization was performed on the f-MWCNT reinforce SPEEK to enhance the cell attachment and cell proliferation as well.

5.1 Structural Analysis of f-MWCNT and SPEEK

Before fabrication of SPEEK/CNT nanocomposite films, its PEEK and CNT were modified to enable their processability via solvent casting and to increase affinity between two PEEK and CNT. Additionally, functionalization of both constituents enhance the biocompatibility and wettability which are desirable characteristics for biomedical application. Moreover, interfacial interaction between carboxyl groups of CNT and sulfonate functional groups in PEEK occurs via strong hydrogen bonding. A good adhesion plays a crucial role in the formation of homogenous nanocomposites increase the miscibility rate of CNT with PEEK and therefore this lead to improvement of the physical properties [69].

CNT has attracted as a reinforcement agent because of its exceptionally high elastic modulus, large surface area and low density. However, its intrinsic nature leads to strong propensity for entanglement. Formation of agglomeration in the matrix prevents fabrication of high quality nanocomposites [20]. Oxidative treatment of CNT with strong acids is one of the ways to increase the dispersibility of CNT within the polymer

matrix by producing hydrophilic functional groups on the defect side. In this study, CNT powder was treated in the H_2SO_4/HNO_3 acid solution to accomplish carboxyl functionalized CNT. After carboxyl group functionalization of MWCNT, to clarify the presence of functional groups were confirmed with FTIR analysis. FTIR spectra shows distinct absorptions bands -COOH groups on the surface which are emerged as a result of oxidative treatment of MWCNT were observed. These peaks at 1770 cm^{-1}, 1390 cm^{-1} 1079 cm^{-1} and 3435 cm^{-1} corresponded the -C=O stretching vibration, -O-H bending vibration, -C-O stretch binding and -O-H stretching binding vibration of the pendant -COOH, respectively [39, 40, 70]. The obtained characteristic bands are in accordance with the literature. Therefore, FTIR data proved the achievement of functional group introduction.

The aromatic backbone of PEEK upholds mechanical and thermal stability of its structure and it allows chemical modification through simple electrophilic substitution by sulfonation. Sulfonation of the PEEK enables its solubility in the organic solvents and increase its hydrophilicity [6]. To prove the sulfonate groups of PEEK and calculate the degree of sulfonation, FTIR and H-NMR were employed. According to FTIR spectra, specific bands appeared at $1254cm^{-1}$, $1076cm^{-1}$, 1020 cm^{-1}, and $708cm^{-1}$ which were corresponding to the sulfonate groups which were in agreement with previous literature reports. The H-NMR data showed the distinct peak for HE proton at 7.50 ppm [71]. This data is also in accordance with the literature result by the similar procedure. The DS of SPEEK was determined as 81% which is quite soluble in common solvent.

5.2 Surface Characterization of Nanofilm

Nanofilms were produced by solvent casting technique by dissolving 10 wt. % of SPEEK in DMF and then blending in subsequently polymer solution was blended with well dispersed 0.5 wt. %, 1wt. % and 2wt. % f-MWCNT. After evaporation of the solvent the nanofilms were obtained. Resultant nanofilms were immobilized with L-arginine in three consecutive steps. Firstly, to generate free NH_2 $1 \times 2cm^2$ with

a thickness of 150±20 μm, samples were immersed in 50% hydrazine monohydrate solution. The primary amine group of hydrazine reacts with ketone groups, which is called a 'ketimine linkage'. Figure 5.1 indicates the formation of ketamine bond.

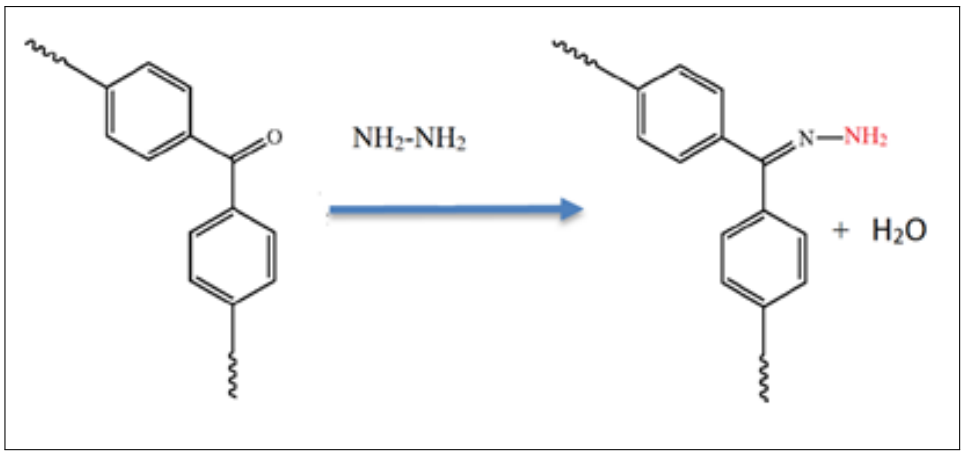

Figure 5.1 Illustration of introduction of primary amine group to SPEEK/CNT nanofilm via formation of ketamine linkages [72].

The second stage of the nanofilms was treatment with GA. This leads to 'Schiff base' chemical reaction where the aldehyde group of GA bonded with NH_2 groups on the nanofilm by yielding bond via $-N = CH - (CH_2)_3CHO$ and one free aldehyde group emerged for further modification [73]. GA also improved the stability of material while enhancing its sterility [14]. Finally, samples were incubated in 2% L-arg solution. L-arg modified nanofilms were obtained via imine bond ($-C = N$) between the residual aldehyde groups of GA and the amino groups of L-arg. Figure shows the reaction carried out [15]. The prepared samples were characterized with XPS, WCA and AFM. XPS was performed to elucidate the elemental composition of the surface and valance states of individual elements. Survey scan of SPEEK/CNT, SPEEK/CNT-NH_2 and SPEEK/CNT-L-arg and C1s and N1s high resolution of SPEEK/CNT-NH_2 and SPEEK/CNT-L-arg were obtained from XPS data. The peak at 400 eV indicates the presence of N atom. Atomic concentration of N sharply increased after L- arg attachment. The photoemission peak at 288.15 eV in the C1s fitting curves was also proved the formation of $-C - NH - C-$ after addition of L-arg [74]. Moreover, the peak at 401.33 eV in the N1s fitting curves is evidence for this new bond [62]. These results verified the success of L-arg modification on the surface of SPEEK/CNT nanofilm covalently which shows similarity with the previous XPS analysis in the literature [57].

To evaluate the surface wettability of modified and unmodified nanofilms, WCA measurements were taken. After concentric H_2SO_4 treatment, water contact angle decreased dramatically which means the sulfonation reaction is pretty effective to elevate hydrophobicity of PEEK [13]. The water contact angle value was 67.77 for SPEEK which was pretty close with the literature [75]. The introduction of f-MWCNT was slightly rised the contact angle of the nanofilms. However, changes were not dramatic as f-MWCNT was in SPEEK polymer matrix rather than on the surface of the films. Nonetheless the lowest contact angle value was for SPEEK/CNT 2. Surface roughness significantly effects for the cellular spreading on the biomaterials. AFM analysis was carried out to determine the surface roughness (Ra) and to investigate the surface morphologies of modified and unmodified films. A more homogenous distribution was observed for SPEEK/CNT 2 than that of the other groups. There was a significant increase in the Ra values, especially SPEEK/CNT 2 nanofilm was the highest with value of 23.60 nm. After L-arg grafting the Ra value was measured as 0.18 μm.

5.3 Mechanical Characterization of Nanofilm

One of the main objectives of this study was to improve the mechanical strength of SPEEK with the addition of MWCNT. The impact of addition of f-MWCNT with three different concentrations on the mechanical behavior was investigated. Temperature variant dynamic mechanical properties and thermal behavior of the nanocomposite films were assessed with DMA analyses in the linear viscoelastic region. Temperature dependent storage modulus and $tan\delta$ was plotted. The obtained graphs demonstrated that the addition of f-MWCNT as a filler significantly influenced the mechanical behavior and Tg values of the films. The storage modulus at 37°C were taken into account for interpretation.

Overall, there was a rise of the storage modulus correlated with the increased CNT rate in the polymer matrix. There was a slight increase in the storage modulus with the rise of wt. % of CNT from 0.5 wt. % to 2 wt. %. The result was attributed to inhomogeneous of the samples. The storage modulus of nanofilm with 2% CNT

additive (2261 MPa) was 1.5 times higher than that of the SPEEK (1500 MPa) [67]. There were several underlying reasons of the higher storage modulus for SPEEK/CNT 2. The most important one is high elastic modulus of CNT leads to rise of storage modulus. Another reason was the formation of strong hydrogen bonds between hydrophilic functional groups which lead to an effective interfacial adhesion for excellent stress transfer. These hydrogen linkages restricts the mobility of the polymer chains that gives rise to achievement of high mechanical strength.

In the DMA curve $tan\delta$ value of the material increased when the nanocomposites reached their glass transition temperature during occurrence of their stress relaxation. The temperature which corresponding to the maximum $tan\delta$ value in the curve is called glass transition (Tg). The Tg value was 162° for SPEEK. The Tg values was above 190° for SPEEK/CNT 1 and SPEEK/CNT 2. As expected, the material structure became more stable with rise of their Tg. However, The Tg values for SPEEK/ CNT 0.5 was below the Tg values of neat polymer.

To sum up, the advanced homogeneous dispersion of f-MWCNT within the polymer matrix was also proven by DMA results. The successful load transfer from matrix to filler accounted for improved modulus.

5.4 Cell Culture Studies

To observe the effect of L-arg and CNT on cellular behavior of hFOB cell, cell culture studies was carried out. The viability on the cell seeded samples was analyzed with Alamar blue after 1^{st} and 3^{rd} days of 48-well plate incubation. At the end of both days there is a similar trend in the experimental groups. Moreover, there was a remarkable increase in the cell viability for each group at the 3^{rd} day of incubation. Addition of f-MWCNT into SPEEK matrix was also slightly increased the cell viability. That could be due to advanced stiffness of CNT modified nanocomposite films. However, cell viability was the highest on the L-arg modified nanofilm. From the obtained results it can be deduced that L-arg biomolecule encouraged cell adhesion

and proliferation significantly. Finally, Alamar blue assay as a quantitative method provides information regarding cell proliferation. In this regard obtained cell culture data shows an acceptable correlation between obtained proliferation percentage and cell doubling time of 36 hours as reported in the literature [76].

5.5 Future Studies

Biological activity of SPEEK, SPEEK/CNT and SPEEK/CNT-L-arg must be investigated elaborately. The duration of viability and proliferation assay will be expanded up to day 7.

REFERENCES

1. Montero, J. F., H. A. Tajiri, G. M. Barra, M. C. Fredel, C. A. Benfatti, R. S. Magini, A. L. Pimenta, and J. C. Souza, "Biofilm behavior on sulfonated poly (ether-ether-ketone)(speek)," *Materials Science and Engineering: C*, Vol. 70, pp. 456–460, 2017.

2. Wang, H., T. Lu, F. Meng, H. Zhu, and X. Liu, "Enhanced osteoblast responses to poly ether ether ketone surface modified by water plasma immersion ion implantation," *Colloids and Surfaces B: Biointerfaces*, Vol. 117, pp. 89–97, 2014.

3. Zheng, Y., C. Xiong, S. Zhang, X. Li, and L. Zhang, "Bone-like apatite coating on functionalized poly (etheretherketone) surface via tailored silanization layers technique," *Materials Science and Engineering: C*, Vol. 55, pp. 512–523, 2015.

4. Ma, R., and T. Tang, "Current strategies to improve the bioactivity of peek," *International Journal of Molecular Sciences*, Vol. 15, no. 4, pp. 5426–5445, 2014.

5. Han, C.-T., M. Chi, Y.-Y. Zheng, L.-X. Jiang, C.-D. Xiong, and L.-F. Zhang, "Mechanical properties and bioactivity of high-performance poly (etheretherketone)/carbon nanotubes/bioactive glass biomaterials," *Journal of Polymer Research*, Vol. 20, no. 8, p. 203, 2013.

6. Tsou, H.-K., P.-Y. Hsieh, C.-J. Chung, C.-H. Tang, T.-W. Shyr, and J.-L. He, "Low-temperature deposition of anatase tio 2 on medical grade polyetheretherketone to assist osseous integration," *Surface and Coatings Technology*, Vol. 204, no. 6, pp. 1121–1125, 2009.

7. Evans, N. T., F. B. Torstrick, C. S. Lee, K. M. Dupont, D. L. Safranski, W. A. Chang, A. E. Macedo, A. S. Lin, J. M. Boothby, D. C. Whittingslow, *et al.*, "High-strength, surface-porous polyether-ether-ketone for load-bearing orthopedic implants," *Acta Biomaterialia*, Vol. 13, pp. 159–167, 2015.

8. Tsou, H.-K., P.-Y. Hsieh, M.-H. Chi, C.-J. Chung, and J.-L. He, "Improved osteoblast compatibility of medical-grade polyetheretherketone using arc ionplated rutile/anatase titanium dioxide films for spinal implants," *Journal of Biomedical Materials Research Part A*, Vol. 100, no. 10, pp. 2787–2792, 2012.

9. Kaczorowski, W., D. Batory, W. Szymanski, and P. Niedzielski, "Evaluation of the surface properties of peek substrate after two-step plasma modification: Etching and deposition of dlc coatings," *Surface and Coatings Technology*, Vol. 265, pp. 92–98, 2015.

10. Díez-Pascual, A. M., M. Naffakh, M. A. Gómez, C. Marco, G. Ellis, M. T. Martínez, A. Ansón, J. M. González-Domínguez, Y. Martínez-Rubi, and B. Simard, "Development and characterization of peek/carbon nanotube composites," *Carbon*, Vol. 47, no. 13, pp. 3079–3090, 2009.

11. Yanmei, J., L. Haihui, W. Ning, H. Lichen, and Z. Xing-Xiang, "Dispersibility and chemical bonds between multi-walled carbon nanotubes and poly (ether ether ketone) in nanocomposite fibers," *Materials Chemistry and Physics*, Vol. 135, no. 2, pp. 948–956, 2012.

12. Yun, S., H. Im, Y. Heo, and J. Kim, "Crosslinked sulfonated poly (vinyl alcohol)/sulfonated multi-walled carbon nanotubes nanocomposite membranes for direct methanol fuel cells," *Journal of Membrane Science*, Vol. 380, no. 1, pp. 208–215, 2011.

13. Miyazaki, T., C. Matsunami, and Y. Shirosaki, "Bioactive carbon–peek composites prepared by chemical surface treatment," *Materials Science and Engineering: C*, Vol. 70, pp. 71–75, 2017.

14. Kim, H. J., J. W. Bae, C. H. Kim, J. W. Lee, J. W. Shin, and K. D. Park, "Acellular matrix of bovine pericardium bound with l-arginine," *Biomedical Materials*, Vol. 2, no. 3, p. S111, 2007.

15. Liu, Y., Y. Yang, and F. Wu, "Effects of l-arginine immobilization on the anticoagulant activity and hemolytic property of polyethylene terephthalate films," *Applied Surface Science*, Vol. 256, no. 12, pp. 3977–3981, 2010.

16. Harris, P. J., "Carbon nanotube composites," *International Materials Reviews*, Vol. 49, no. 1, pp. 31–43, 2004.

17. Uthamalingam, P., and S. Mehta, "Crystal-storing histiocytosis: Report of a rare case presenting with pathological fracture of femur. is there more to the entity?," *International Journal of Surgical Pathology*, p. 1066896917696746, 2017.

18. Pino, M., W. Chrzanowski, D. Fabel, M. Baklar, N. Stingelin, and K. E. Tanner, "Apatite deposition on naoh-treated peek and uhmwpe films for sclera materials in artificial cornea implants," *Advanced Engineering Materials*, Vol. 12, no. 7, 2010.

19. Khan, F., and S. R. Ahmad, "Bioactive polymers and nanobiomaterials composites for bone tissue engineering," *Biomimetics: Advancing Nanobiomaterials and Tissue Engineering*, pp. 91–117, 2013.

20. Cao, Z., L. Qiu, Y. Yang, Y. Chen, and X. Liu, "The surface modifications of multi-walled carbon nanotubes for multi-walled carbon nanotube/poly (ether ether ketone) composites," *Applied Surface Science*, Vol. 353, pp. 873–881, 2015.

21. Choudhary, V., B. Singh, and R. Mathur, "Carbon nanotubes and their composites," in *Syntheses and applications of carbon nanotubes and their composites*, InTech, 2013.

22. Nayak, T. R., L. Jian, L. C. Phua, H. K. Ho, Y. Ren, and G. Pastorin, "Thin films of functionalized multiwalled carbon nanotubes as suitable scaffold materials for stem cells proliferation and bone formation," *ACS nano*, Vol. 4, no. 12, pp. 7717–7725, 2010.

23. Sathyanarayana, S., and C. Hübner, "Thermoplastic nanocomposites with carbon nanotubes," in *Structural Nanocomposites*, pp. 19–60, Springer, 2013.

24. Shah, A. H., "Applications of carbon nanotubes and their polymer nanocomposites for gas sensors," in *Carbon Nanotubes-Current Progress of their Polymer Composites*, InTech, 2016.

25. Zhang, Y., Y. Bai, and B. Yan, "Functionalized carbon nanotubes for potential medicinal applications," *Drug Discovery Today*, Vol. 15, no. 11, pp. 428–435, 2010.

26. Balasubramanian, K., and M. Burghard, "Chemically functionalized carbon nanotubes," *Small*, Vol. 1, no. 2, pp. 180–192, 2005.

27. He, H., L. A. Pham-Huy, P. Dramou, D. Xiao, P. Zuo, and C. Pham-Huy, "Carbon nanotubes: applications in pharmacy and medicine," *BioMed Research International*, Vol. 2013, 2013.

28. Marshall, M. W., S. Popa-Nita, and J. G. Shapter, "Measurement of functionalised carbon nanotube carboxylic acid groups using a simple chemical process," *Carbon*, Vol. 44, no. 7, pp. 1137–1141, 2006.

29. Mou'ad, A. T., and S. H. Ahmad, "Characterization and morphology of modified multi-walled carbon nanotubes filled thermoplastic natural rubber (tpnr) composite," in *Syntheses and Applications of Carbon Nanotubes and Their Composites*, InTech, 2013.

30. Sahoo, N. G., S. Rana, J. W. Cho, L. Li, and S. H. Chan, "Polymer nanocomposites based on functionalized carbon nanotubes," *Progress in polymer science*, Vol. 35, no. 7, pp. 837–867, 2010.

31. Zhao, X., and R. Liu, "Recent progress and perspectives on the toxicity of carbon nanotubes at organism, organ, cell, and biomacromolecule levels," *Environment International*, Vol. 40, pp. 244–255, 2012.

32. Vardharajula, S., S. Z. Ali, P. M. Tiwari, E. Eroğlu, K. Vig, V. A. Dennis, and S. R. Singh, "Functionalized carbon nanotubes: biomedical applications," *International Journal of Nanomedicine*, Vol. 7, p. 5361, 2012.

33. Faria, P. C. B. d., L. I. d. Santos, J. P. Coelho, H. B. Ribeiro, M. A. Pimenta, L. O. Ladeira, D. A. Gomes, C. A. Furtado, and R. T. Gazzinelli, "Oxidized multiwalled carbon nanotubes as antigen delivery system to promote superior cd8+ t cell response and protection against cancer," *Nano Letters*, Vol. 14, no. 9, pp. 5458–5470, 2014.

34. Boaretti, C., M. Roso, A. Lorenzetti, and M. Modesti, "Synthesis and process optimization of electrospun peek-sulfonated nanofibers by response surface methodology," *Materials*, Vol. 8, no. 7, pp. 4096–4117, 2015.

35. Rong, C., G. Ma, S. Zhang, L. Song, Z. Chen, G. Wang, and P. Ajayan, "Effect of carbon nanotubes on the mechanical properties and crystallization behavior of poly (ether ether ketone)," *Composites Science and Technology*, Vol. 70, no. 2, pp. 380–386, 2010.

36. Fatarella, E., V. Mylläri, M. Ruzzante, R. Pogni, M. C. Baratto, M. Skrifvars, S. Syrjälä, and P. Järvelä, "Sulfonated polyetheretherketone/polypropylene polymer blends for the production of photoactive materials," *Journal of Applied Polymer Science*, Vol. 132, no. 8, 2015.

37. Nagiah, N., L. Madhavi, R. Anitha, C. Anandan, N. T. Srinivasan, and U. T. Sivagnanam, "Development and characterization of coaxially electrospun gelatin coated poly (3-hydroxybutyric acid) thin films as potential scaffolds for skin regeneration," *Materials Science and Engineering: C*, Vol. 33, no. 7, pp. 4444–4452, 2013.

38. Parra, J., I. H. García Páez, A. H. De Aza, C. Baudin, M. Rocío Martín, and P. Pena, "In vitro study of the proliferation and growth of human fetal osteoblasts on mg and si co-substituted tricalcium phosphate ceramics," *Journal of Biomedical Materials Research Part A*, 2017.

39. Wang, J., Z. Li, S. Li, W. Qi, P. Liu, F. Liu, Y. Ye, L. Wu, L. Wang, and W. Wu, "Adsorption of cu (ii) on oxidized multi-walled carbon nanotubes in the presence of hydroxylated and carboxylated fullerenes," *PloS one*, Vol. 8, no. 8, p. e72475, 2013.

40. Madani, S. Y., A. Tan, M. Dwek, and A. M. Seifalian, "Functionalization of single-walled carbon nanotubes and their binding to cancer cells," *International Journal of Nanomedicine*, Vol. 7, p. 905, 2012.

41. Nawaz, M. A. H., S. Rauf, G. Catanante, M. H. Nawaz, G. Nunes, J. L. Marty, and A. Hayat, "One step assembly of thin films of carbon nanotubes on screen printed interface for electrochemical aptasensing of breast cancer biomarker," *Sensors*, Vol. 16, no. 10, p. 1651, 2016.

42. Safari, J., and S. Gandomi-Ravandi, "Fe 3 o 4–cnts nanocomposites: a novel and excellent catalyst in the synthesis of diarylpyrimidinones using grindstone chemistry," *RSC Advances*, Vol. 4, no. 22, pp. 11486–11492, 2014.

43. Mphuthi, N. G., A. S. Adekunle, and E. E. Ebenso, "Electrocatalytic oxidation of epinephrine and norepinephrine at metal oxide doped phthalocyanine/mwcnt composite sensor," *Scientific reports*, Vol. 6, p. 26938, 2016.

44. Her, S.-C., and C.-Y. Lai, "Dynamic behavior of nanocomposites reinforced with multi-walled carbon nanotubes (mwcnts)," *Materials*, Vol. 6, no. 6, pp. 2274–2284, 2013.

45. Tan, J. M., G. Karthivashan, P. Arulselvan, S. Fakurazi, and M. Z. Hussein, "Characterization and in vitro sustained release of silibinin from ph responsive carbon nanotube-based drug delivery system," *Journal of Nanomaterials*, Vol. 2014, p. 1, 2014.

46. Li, Y., M. Zhang, X. Wang, Z. Li, and L. Zhao, "Anhydrous conducting composite membranes composed of speek/silica/ionic liquids for high-temperature proton exchange," *Electrochimica Acta*, Vol. 222, pp. 1308–1315, 2016.

47. Leong, J. X., W. R. W. Daud, M. Ghasemi, A. Ahmad, M. Ismail, and K. B. Liew, "Composite membrane containing graphene oxide in sulfonated polyether ether ketone in microbial fuel cell applications," *International Journal of Hydrogen Energy*, Vol. 40, no. 35, pp. 11604–11614, 2015.

48. Al Lafi, A. G., "The sulfonation of poly (ether ether ketone) as investigated by two-dimensional ftir correlation spectroscopy," *Journal of Applied Polymer Science*, Vol. 132, no. 2, 2015.

49. Inan, T. Y., H. Doğan, E. E. Unveren, and E. Eker, "Sulfonated peek and fluorinated polymer based blends for fuel cell applications: investigation of the effect of type and molecular weight of the fluorinated polymers on the membrane's properties," *International Journal of Hydrogen Energy*, Vol. 35, no. 21, pp. 12038–12053, 2010.

50. Tsai, J.-C., H.-P. Cheng, J.-F. Kuo, Y.-H. Huang, and C.-Y. Chen, "Blended nafion®/speek direct methanol fuel cell membranes for reduced methanol permeability," *Journal of Power Sources*, Vol. 189, no. 2, pp. 958–965, 2009.

51. Koziara, B. T., E. J. Kappert, W. Ogieglo, K. Nijmeijer, M. A. Hempenius, and N. E. Benes, "Thermal stability of sulfonated poly (ether ether ketone) films: on the role of protodesulfonation," *Macromolecular Materials and Engineering*, Vol. 301, no. 1, pp. 71–80, 2016.

52. Rahnavard, A., S. Rowshanzamir, M. J. Parnian, and G. R. Amirkhanlou, "The effect of sulfonated poly (ether ether ketone) as the electrode ionomer for self-humidifying nanocomposite proton exchange membrane fuel cells," *Energy*, Vol. 82, pp. 746–757, 2015.

53. Wu, H.-L., C.-C. M. Ma, F.-Y. Liu, C.-Y. Chen, S.-J. Lee, and C.-L. Chiang, "Preparation and characterization of poly (ether sulfone)/sulfonated poly (ether ether ketone) blend membranes," *European Polymer Journal*, Vol. 42, no. 7, pp. 1688–1695, 2006.

54. Muthu, R. N., S. Rajashabala, and R. Kannan, "Synthesis and characterization of polymer (sulfonated poly-ether-ether-ketone) based nanocomposite (h-boron nitride) membrane for hydrogen storage," *International Journal of Hydrogen Energy*, Vol. 40, no. 4, pp. 1836–1845, 2015.

55. Zhang, W., H. Huang, F. Li, K. Deng, and X. Wang, "Palladium nanoparticles supported on graphitic carbon nitride-modified reduced graphene oxide as highly efficient catalysts for formic acid and methanol electrooxidation," *Journal of Materials Chemistry A*, Vol. 2, no. 44, pp. 19084–19094, 2014.

56. Eby, D. M., K. Artyushkova, A. K. Paravastu, and G. R. Johnson, "Probing the molecular structure of antimicrobial peptide-mediated silica condensation using x-ray photoelectron spectroscopy," *Journal of Materials Chemistry*, Vol. 22, no. 19, pp. 9875–9883, 2012.

57. Zhu, B., P. Xia, W. Ho, and J. Yu, "Isoelectric point and adsorption activity of porous gc 3 n 4," *Applied Surface Science*, Vol. 344, pp. 188–195, 2015.

58. Wang, A., W. Yu, Z. Huang, F. Zhou, J. Song, Y. Song, L. Long, M. P. Cifuentes, M. G. Humphrey, L. Zhang, *et al.*, "Covalent functionalization of reduced graphene oxide with porphyrin by means of diazonium chemistry for nonlinear optical performance," *Scientific Reports*, Vol. 6, p. 23325, 2016.

59. Mahjoubi, H., E. Buck, P. Manimunda, R. Farivar, R. Chromik, M. Murshed, and M. Cerruti, "Surface phosphonation enhances hydroxyapatite coating adhesion on polyetheretherketone and its osseointegration potential," *Acta Biomaterialia*, Vol. 47, pp. 149–158, 2017.

60. Liu, Z., X. Duan, G. Qian, X. Zhou, and W. Yuan, "Eco-friendly one-pot synthesis of highly dispersible functionalized graphene nanosheets with free amino groups," *Nanotechnology*, Vol. 24, no. 4, p. 045609, 2013.

61. Han, H., G. Ding, T. Wu, D. Yang, T. Jiang, and B. Han, "Cu and boron doped carbon nitride for highly selective oxidation of toluene to benzaldehyde," *Molecules*, Vol. 20, no. 7, pp. 12686–12697, 2015.

62. Zhou, W., Y. Zhou, L. Yang, J. Huang, Y. Ke, K. Zhou, L. Li, and S. Chen, "N-doped carbon-coated cobalt nanorod arrays supported on a titanium mesh as highly active electrocatalysts for the hydrogen evolution reaction," *Journal of Materials Chemistry A*, Vol. 3, no. 5, pp. 1915–1919, 2015.

63. Di Vona, M. L., E. Sgreccia, R. Narducci, L. Pasquini, H. Hou, and P. Knauth, "Stabilized sulfonated aromatic polymers by in situ solvothermal cross-linking," *Frontiers in Energy Research*, Vol. 2, p. 39, 2014.

64. Sgreccia, E., J.-F. Chailan, M. Khadhraoui, M. Di Vona, and P. Knauth, "Mechanical properties of proton-conducting sulfonated aromatic polymer membranes: stress–strain tests and dynamical analysis," *Journal of Power Sources*, Vol. 195, no. 23, pp. 7770–7775, 2010.

65. Di Vona, M., E. Sgreccia, A. Donnadio, M. Casciola, J. Chailan, G. Auer, and P. Knauth, "Composite polymer electrolytes of sulfonated poly-ether-ether-ketone (speek) with organically functionalized tio 2," *Journal of Membrane Science*, Vol. 369, no. 1, pp. 536–544, 2011.

66. Heo, Y., H. Im, and J. Kim, "The effect of sulfonated graphene oxide on sulfonated poly (ether ether ketone) membrane for direct methanol fuel cells," *Journal of Membrane Science*, Vol. 425, pp. 11–22, 2013.

67. Vinothkannan, M., A. R. Kim, K. S. Nahm, and D. J. Yoo, "Ternary hybrid (speek/spvdf-hfp/go) based membrane electrolyte for the applications of fuel cells: profile of improved mechanical strength, thermal stability and proton conductivity," *RSC Advances*, Vol. 6, no. 110, pp. 108851–108863, 2016.

68. Wilberforce, S. I., C. E. Finlayson, S. M. Best, and R. E. Cameron, "A comparative study of the thermal and dynamic mechanical behaviour of quenched and annealed bioresorbable poly-l-lactide/α-tricalcium phosphate nanocomposites," *Acta biomaterialia*, Vol. 7, no. 5, pp. 2176–2184, 2011.

69. Song, R., D. Yang, and L. He, "Preparation of semi-aromatic polyamide (pa)/multi-wall carbon nanotube (mwcnt) composites and its dynamic mechanical properties," *Journal of Materials Science*, Vol. 43, no. 4, pp. 1205–1213, 2008.

70. Fraczek-Szczypta, A., E. Menaszek, T. B. Syeda, A. Misra, M. Alavijeh, J. Adu, and S. Blazewicz, "Effect of mwcnt surface and chemical modification on in vitro cellular response," *Journal of Nanoparticle Research*, Vol. 14, no. 10, p. 1181, 2012.

71. Xing, P., G. P. Robertson, M. D. Guiver, S. D. Mikhailenko, K. Wang, and S. Kaliaguine, "Synthesis and characterization of sulfonated poly (ether ether ketone) for proton exchange membranes," *Journal of Membrane Science*, Vol. 229, no. 1, pp. 95–106, 2004.

72. Yuan, Y., and Y. Ding, "Functionalized porous poly(aryl ether ketone) materials and their use," 2007. US Patent 7,176,273.

73. Wang, L.-Y., Y.-J. Wang, and D.-R. Cao, "Surface modification of poly (3-hydroxybutyrate-co-3-hydroxyvalerate) membrane by combining surface aminolysis treatment with collagen immobilization," *Journal of Macromolecular Science®, Part A: Pure and Applied Chemistry*, Vol. 46, no. 8, pp. 765–773, 2009.

74. Liao, C. Z., K. Li, H. M. Wong, W. Y. Tong, K. W. K. Yeung, and S. C. Tjong, "Novel polypropylene biocomposites reinforced with carbon nanotubes and hydroxyapatite nanorods for bone replacements," *Materials Science and Engineering: C*, Vol. 33, no. 3, pp. 1380–1388, 2013.

75. James, R., R. K. Nagarale, V. K. Sachan, C. Badalucco, P. K. Bhattacharya, and S. G. Kumbar, "Synthesis and characterization of electrically conducting polymers for regenerative engineering applications: sulfonated ionic membranes," *Polymers for Advanced Technologies*, Vol. 25, no. 12, pp. 1439–1445, 2014.

76. Montjovent, M.-O., N. Burri, S. Mark, E. Federici, C. Scaletta, P.-Y. Zambelli, P. Hohlfeld, P.-F. Leyvraz, L. L. Applegate, and D. P. Pioletti, "Fetal bone cells for tissue engineering," *Bone*, Vol. 35, no. 6, pp. 1323–1333, 2004.